


Timing and evolution of Middle Triassic magmatism in the Southern Alps (northern Italy)

Julian-Christopher Storck*, Peter Brack, Jörn-Frederik Wotzlaw & Peter Ulmer

Institute of Geochemistry and Petrology, Department of Earth Sciences, ETH Zurich, Clausiusstrasse 25, Zurich, Switzerland

 J.-C.S., 0000-0003-4438-4061; J.-F.W., 0000-0003-3363-7764

* Correspondence: julian.storck@erdw.ethz.ch



Abstract: Middle Triassic magmatism in the Southern Alps (northern Italy) consists of widespread volcanoclastic deposits, basaltic lava flows and intrusive complexes. Despite their importance in understanding the geodynamic evolution of the westernmost Tethys, the timing of magmatic activity and the links between the different igneous products remain poorly understood. We present a comprehensive high-precision zircon U–Pb geochronology dataset for the major intrusive complexes and several volcanic ash layers and integrate this with a high-resolution stratigraphic framework of Middle Triassic volcano-sedimentary successions. The main interval of Middle Triassic magmatism lasted at least 5.07 ± 0.06 myr. Magmatic activity started with silicic eruptions between 242.653 ± 0.036 and 238.646 ± 0.037 Ma, followed by a <1 myr eruptive interval of voluminous basaltic lava flows. Coeval mafic to intermediate intrusions dated at 238.190 ± 0.055 to 238.075 ± 0.087 Ma may represent feeder and subvolcanic complexes related to the basalt flows. The youngest products are silicic tuffs from latest Ladinian to early Carnian sequences dated at 237.680 ± 0.047 and 237.579 ± 0.042 Ma. Complemented by zircon trace element data, our high-resolution temporal framework places tight constraints on the link between silicic and mafic igneous products in a complex geodynamic setting.

Supplementary material: Isotope dilution thermal ionization mass spectrometry U–Pb and laser ablation inductively coupled plasma mass spectrometry trace element data tables, sample coordinates, supplementary geochemical data, cathodoluminescence images of isotope dilution thermal ionization mass spectrometry dated zircons and supplementary field documentation are available at <https://doi.org/10.6084/m9.figshare.c.4287506>

Received 17 June 2018; revised 26 October 2018; accepted 1 November 2018

The timing, duration and distribution of volcanic and intrusive products are characteristic features of magmatic provinces and allow igneous activity to be placed into a tectonic framework. Middle Triassic magmatism in the Southern Alps consists of widespread felsic volcanoclastic deposits, basaltic lava flows and irregularly distributed intrusive complexes. The origin and petrogenesis of this magmatic flare-up, as well as the temporal and genetic relationships between volcanic and intrusive products, remain poorly understood. The tectonic settings proposed for this magmatic activity range from rifting to large-scale strike-slip and subduction scenarios (see [Abbas *et al.* 2018](#) for a recent summary). Available U–Pb zircon ages and biochronological constraints from the Southern Alps ([Brack *et al.* 2007](#) and references cited therein; [Mietto *et al.* 2012](#)) suggest that the duration of the main magmatic interval was short (<6 myr, from *c.* 243.3 to 237.77 Ma).

Of particular importance for this temporal calibration is the widespread occurrence of felsic volcanic ash layers in well-studied Middle Triassic fossiliferous sedimentary successions of the Buchenstein Formation, especially in the Lombardian Alps and the Dolomites of northern Italy ([Fig. 1](#)). Such ash layers can be traced over hundreds of kilometres and have previously been used to calibrate the stratigraphic record ([Brack & Rieber 1993](#); [Mundil *et al.* 1996](#)), including the Global Boundary Stratotype Section and Point (GSSP) of the base of the Ladinian Stage ([Brack *et al.* 2005](#)). New high-precision zircon U–Pb geochronology of several volcanic ash beds by [Wotzlaw *et al.* \(2018\)](#) provide a significant refinement for a restricted interval of this chronostratigraphic framework, with a temporal resolution of individual age data below the per mil level. These precise new age data have allowed a re-evaluation of the interpretation of stratigraphic patterns. However, such data also serve

as essential constraints for the detailed reconstruction of magmatic evolution. The much improved level of geochronological resolution not only promises a better understanding of short-lived magmatic events and processes inside a single magmatic unit ([Schoene *et al.* 2012](#); [Wotzlaw *et al.* 2013](#); [Samperton *et al.* 2015](#)), but also provides new opportunities to quantify processes in rapidly evolving settings where magmatism and tectonic structures are found in a well-established stratigraphic context. With spectacularly exposed carbonate platforms, basinal sediments, plutonic and volcanic products and synsedimentary tectonic structures, the Middle Triassic of the Southern Alps, and the Dolomites in particular (e.g. [Bosellini *et al.* 2003](#)), are an ideal test ground for the application of state-of-the-art geochronology to constrain the evolution of a highly dynamic geological setting in unprecedented detail.

We present here a comprehensive high-precision zircon U–Pb geochronology dataset for 12 silicic volcanic ash beds and two intrusive complexes in the Southern Alps. The ash data provide a significant extension of the recalibrated stratigraphic record of [Wotzlaw *et al.* \(2018\)](#) and allow the episode of Triassic magmatism in the Southern Alps to be much better constrained ([Fig. 2](#)). In the Dolomites, the ash beds further bracket the main interval of voluminous basalt eruptions ([Figs 2–6](#)). New data from supposedly coeval and related plutonic and subvolcanic bodies serve as a firm basis for the integration of geochemical data for the well-known Middle Triassic magmatic system in the western Dolomites.

The resulting chronostratigraphic framework is augmented by zircon trace element geochemistry and allows us to place first-order constraints on the temporal and genetic relationships of the silicic explosive and mafic intrusive/effusive magmatism in the Southern Alps during the Middle Triassic.

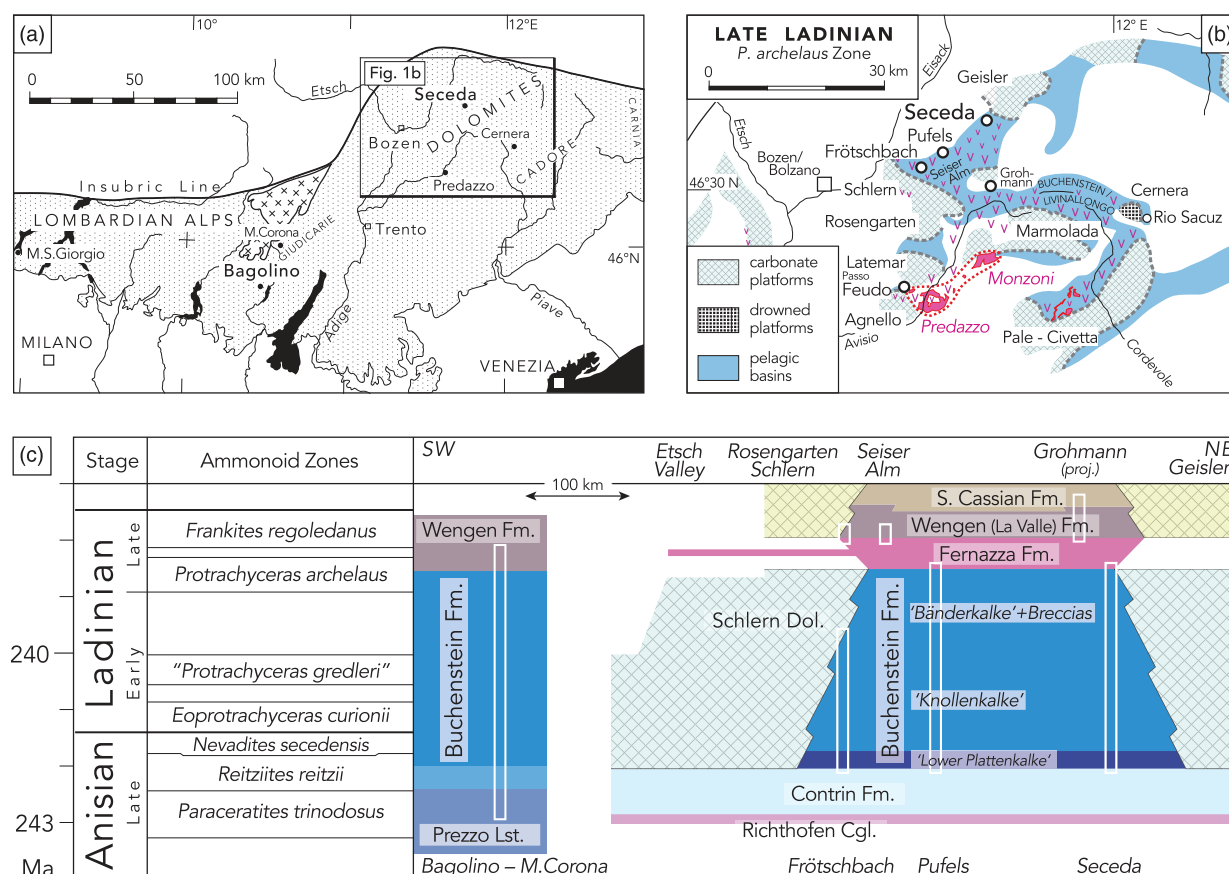


Fig. 1. (a) Overview map of the central and western Southern Alps showing the location of the Bagolino reference section in Eastern Lombardy and the location of the map in part (b). (b) Distribution of high-relief carbonate platforms and deep basins in the central and western Dolomites during the early Ladinian. These basins were subsequently filled by volcanic products (v) and reworked volcanic debris. The locations of the main intrusive centres (Predazzo, Monzoni) are indicated. (c) Chronostratigraphic scheme for the main formations in eastern Lombardy (Bagolino) and in the northwestern Dolomites (modified after Wotzlaw *et al.* 2018). White bars mark the stratigraphic intervals investigated in this study.

Geological setting and distribution of Triassic volcanic rocks and subvolcanic igneous centres

Tectonic framework

The Southern Alps are a major portion of the Alpine edifice south of the Insubric Line and extend over several hundred kilometres throughout northern Italy and southern Switzerland. They represent a south-vergent fold and thrust belt, the transport direction of which was only slightly oblique to major divides resulting from the formation of a passive continental margin in this realm during the latest Triassic to Jurassic (e.g. Bertotti *et al.* 1993; Berra & Carminati 2010). The original stratigraphic relationships of Mesozoic rocks are thus largely preserved in east–west transects along the Southern Alps, or can be reconstructed with confidence. Apart from local phenomena around younger intrusions, the post-Carboniferous rocks of the Southern Alps did not experience any regional metamorphic overprinting during the Alpine orogeny.

The western Dolomites correspond to a large uplifted portion of the Southern Alps and show only relatively mild internal deformation of Alpine age. They display a particularly complex stratigraphic framework, including Middle Triassic carbonate platforms, basinal sediments, emersion horizons, volcanic successions and shallow intrusions (Fig. 1; Bosellini *et al.* 2003). Several pulses of Middle Triassic uplift, accelerated subsidence and strike-slip movements contributed to the formation of the now so spectacularly exposed setting of largely coeval, but very different rocks. Similar successions in other parts of the Southern Alps are found in largely south- to southeast-thrust and partly superposed

units. Nevertheless, the original large-scale stratigraphic pattern is still preserved along-strike in the Southern Alps (Brack & Rieber 1993, their figure 2).

Triassic magmatic products

Igneous rocks and debris from Triassic magmatism are known from numerous places throughout the Southern Alps. Plutonic rocks of shallow intrusions and volcanic lithologies occur in spatially restricted magmatic centres, whereas thin volcanoclastic ash layers are much more widespread (e.g. Assereto *et al.* 1977; Brack & Rieber 1993). The age of the main Triassic magmatic activities as documented in the Southern Alps ranges from Late Anisian to Carnian. These magmatic products can be grouped into three domains and corresponding time intervals. The first domain of Late Anisian to early Ladinian magmatic products is found as variably thick acidic volcanoclastic layers in basinal sediments throughout the entire Southern Alps (Brack & Rieber 1993; Brack *et al.* 2007; Stockar *et al.* 2012). Thin ash layers occasionally also occur in platform carbonates (Mundil *et al.* 2003). The volcanic sources of these debris may have been located elsewhere, but possibly age-equivalent small magmatic centres are also known from the Southern Alps – for example in eastern Lombardy, in the Vicenza pre-Alps and in the northeasternmost Southern Alps (at Friuli). The second domain of predominantly mafic magmatic rocks of Late Ladinian age occur throughout the eastern Southern Alps, with a well-known main magmatic centre in the Dolomites, where voluminous piles of effusive and intrusive basalt accompany

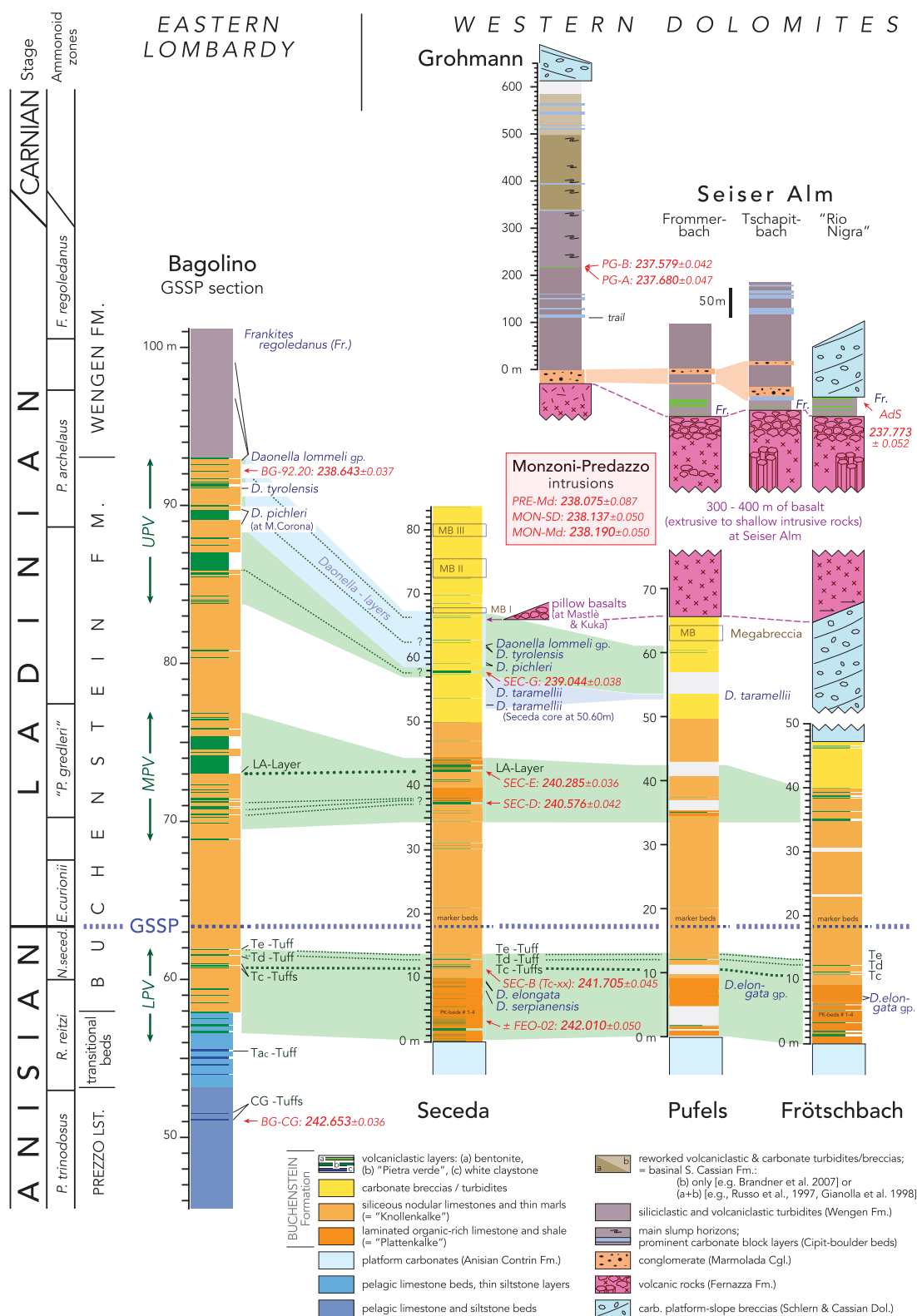


Fig. 2. Stratigraphic correlation scheme of volcanosedimentary key sections hosting the Middle Triassic Buchenstein Formation between Eastern Lombardy and the Dolomites. The sample horizons of volcanic ash beds discussed in this study are labelled in red. The stratigraphic columns for Bagolino and Seceda are modified after Brack & Rieber 1993 with the recalibrated metre scale of Wotzlaw *et al.* (2018) for Seceda and a re-measured log scale for Bagolino. For further details, see text. Alpe di Siusi (AdS) indicates the position of the zircon age of Mietto *et al.* (2012).

the shallow intrusions and possible magmatic conduits of Monzoni–Predazzo (Casetta *et al.* 2018). Small volumes of possibly Late Ladinian mafic magmatic products also occur in eastern Lombardy (Cassinis *et al.* 2008). The third domain is not included in the present study, but consists of largely Carnian magmatic

products, including thin ash layers, in possibly Lower Carnian carbonates (Assereto *et al.* 1977), explosion breccias at roughly the same stratigraphic level (Jadoul *et al.* 2012) and younger voluminous delta systems (Lower/Middle Carnian?) with volcanic-rich sandstones in the Lombardian sector (Garzanti 1985).

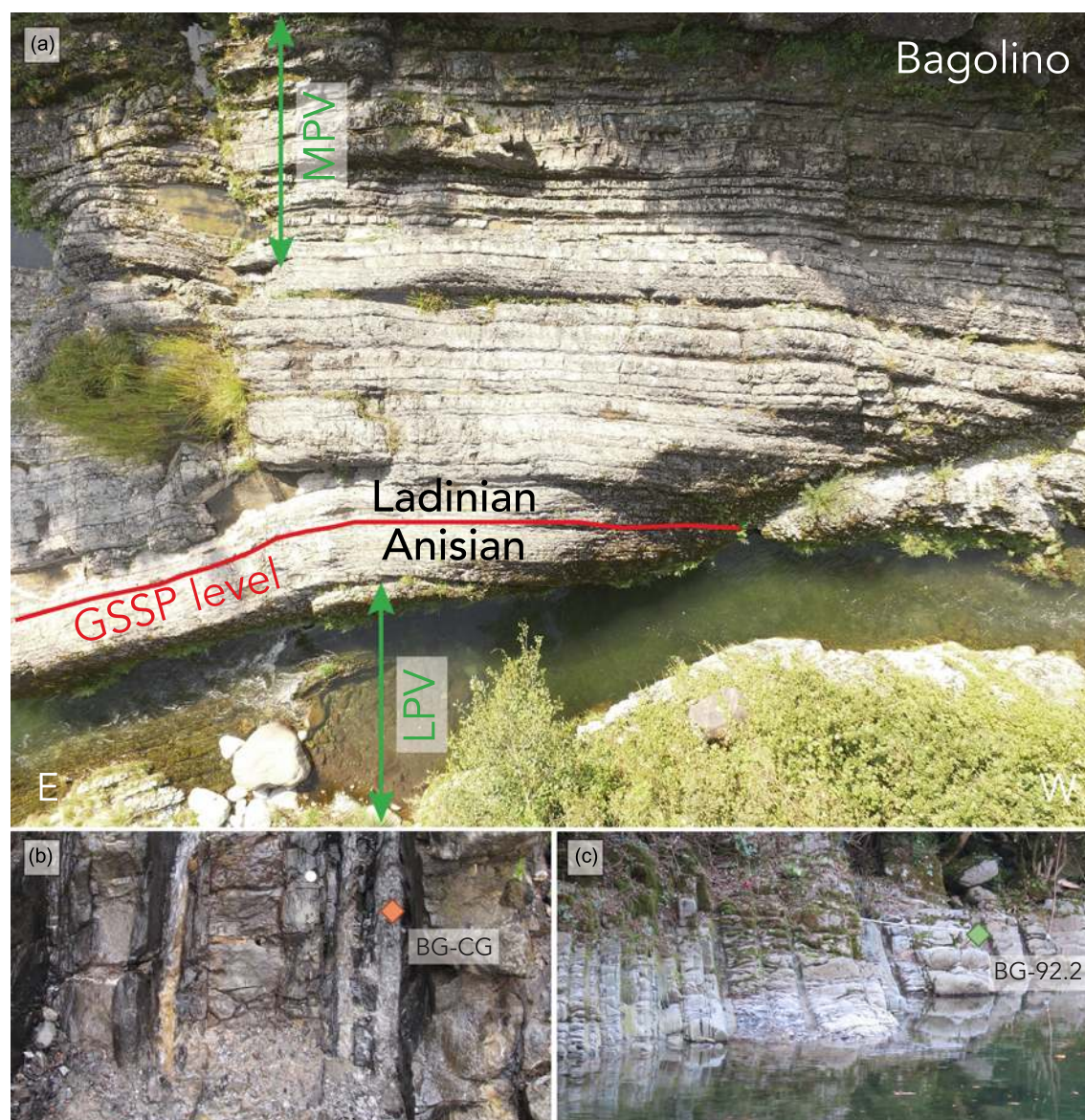


Fig. 3. (a) Aerial view of the vertically oriented Buchenstein Formation, intercalated by Pietra Verde layers (Lower Pietra Verde (LPV) and Middle Pietra Verde (MPV), shown here) at the Bagolino Global Boundary Stratotype Section and Point section. (b) Photograph of the lowermost ash beds in the uppermost Prezzo Limestone (three whitish layers, ‘Contrada Gobbia tuffs’). These are the oldest known records of explosive volcanic activity. (c) View of the Upper Pietra Verde (UPV) interval with the dated ash layer BG-92.2 predating the effusive basalts and the intrusions of Predazzo and Monzoni (see Figs 5 and 6).

Older and/or coeval magmatic centres located further south with mafic to intermediate rocks are known from the area north and northeast of Brescia (Cassinis *et al.* 2008).

Triassic magmatic products may also occur in the deep crustal rocks of the Ivrea–Verbano zone of the westernmost Southern Alps (Zanetti *et al.* 2016) and along a Triassic high in the subsurface of the present Po Plain to the south of the Southern Alps (Brusca *et al.* 1981). An example of a probably Middle Triassic intrusive complex is known from the northern Karawanks (Eisenkappel; Miller *et al.* 2011). Igneous products of Triassic age also occur in the southeastern continuation of the Southern Alps throughout the Dinarides and beyond (e.g. Bébien *et al.* 1978).

Petrological characteristics of Anisian–Ladinian igneous products

The early acidic phase is mainly composed of various types of tephra, ranging from ignimbrites to redeposited volcanoclastics and associated subvolcanic stocks and laccoliths. These rocks contain phenocrysts of alkali feldspar, plagioclase and minor biotite

(Callegari & Monese 1964; Spadea 1970; Obenholzner 1991). The main masses of basaltic to intermediate, rarely felsic, lavas and associated subvolcanic complexes have been studied throughout the Southern Alps.

The basalts (shoshonites) and intermediate rocks (trachyandesites) contain olivine or orthopyroxene and clinopyroxene as the principal phenocryst phases, accompanied by subordinate plagioclase and rare amphibole. The intermediate rocks lack olivine, but K-feldspar appears in the matrix. The latites to trachytes contain plagioclase, K-feldspar, amphibole and biotite, whereas the rhyolites contain resorbed quartz, plagioclase, sanidine and biotite phenocrysts. All rocks are characterized by the high K_2O and high K_2O/Na_2O ratios typical of the shoshonite suite (Sacerdoti & Sommarivilla 1962; De Vecchi & Sedeà 1983; Gasparotto & Simboli 1991; Obenholzner 1991; Casetta *et al.* 2018).

The volcanic ash layers (the so-called Pietra Verde) intercalated with Middle Triassic sediments and *in situ* volcanic rocks of the Prezzo Limestone, Buchenstein Formation and Wengen Formation are suitable for a detailed zircon petrochronological study of the evolution and duration of igneous activity. Ash layers, crystal-rich

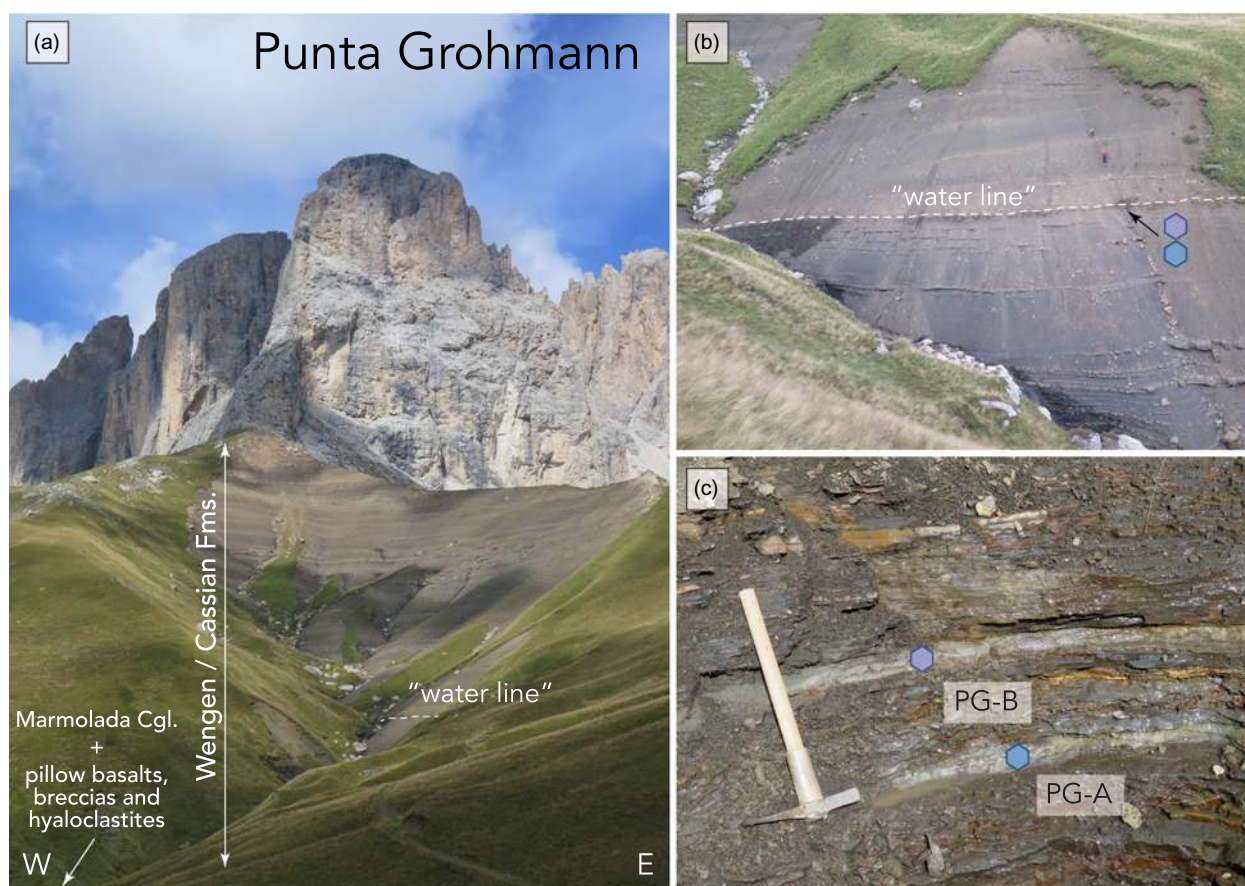


Fig. 4. (a) Illustration of the Punta Grohmann section hosting the (b, c) Wengen Formation intercalated by the two youngest sampled ash beds PG-A and PG-B, marked by a 'water line' indicating the trace of the water-soaked thin bentonite horizons. The Wengen Formation at the Punta Grohmann section directly overlies the Marmolada Conglomerate following on top of *in situ* volcanics (pillow basalts, pillow breccias and hyaloclastites), indicated by the white arrow.

tuffs and bentonites can be observed in stratigraphic sequences throughout the Southern Alps.

More mafic products occur further up-section in the form of shallow intrusions, associated with dykes, basaltic lava flows, pillow lavas, breccias and hyaloclastites. Stratigraphically unconstrained shoshonitic intrusive and effusive bodies, including those of Mt Monzoni and Predazzo, were emplaced in the central and western Dolomites during the late stages of volcanic activity.

Studied sections and lithologies

Volcaniclastic materials from stratigraphically well-constrained and well-correlated successions in eastern Lombardy (Bagolino) and the Dolomites (Seceda, Pufels and Frötschbach) were sampled to establish the duration of the Late Anisian to Ladinian Stage of explosive acidic volcanic activity (Fig. 1). Samples from ash layers at stratigraphically higher levels in the Dolomites (Seiser Alm and Grohmann) constrain the main stage of voluminous basalt eruptions in the central and northwestern Dolomites. Samples were selected from the igneous complex at Monzoni–Predazzo to provide information on the timing of magma emplacement in possible conduits.

Bagolino: positions of dated samples and correlation of data from Seceda

The stratigraphic succession at Bagolino (Fig. 2) has been studied in detail over the past four decades, in particular for its biostratigraphy and volcanic layers (for a description and location of the section, palaeontological information and further references, see Brack *et al.*

2005). The section hosts the GSSP of the base of the Ladinian Stage. About 60 volcanic ash layers can be identified over 40 m of stratigraphic thickness of the uppermost Prezzo Limestone and in the Buchenstein Formation in the pelagic carbonate succession. As a result of their sometimes intense green colour, such layers are referred to as Pietra Verde and occur at higher frequencies in three intervals (the Lower, Middle and Upper Pietra Verde). Two samples from the Bagolino succession (Fig. 3) constrain the interval of explosive silicic eruptions that predate the basaltic lava flows. Sample BG-CG (Bagolino Site A, Brack *et al.* 2005) is from the lowermost of three centimetre-thick, whitish illitic claystones of volcanic origin in the upper Prezzo Limestone. These so-called Contrada Gobbia tuffs are the oldest known volcanic products in pelagic carbonate sections throughout eastern Lombardy. They always occur around the *Asseretoceras camunum* ammonoid horizon and show a wide areal distribution (e.g. Brack & Rieber 1993; Balini & Renesto 2012). At presumably similar stratigraphic positions in sections in the eastern Dolomites, medium-grained volcaniclastic layers are also known from the Bivera Formation (Brack *et al.* 2007). These layers represent the oldest records of Middle Triassic magmatic activity in the South Alpine domain.

Sample BG-92.2 (Bagolino Site B, Brack *et al.* 2005) is from the topmost Buchenstein Formation at Bagolino (Fig. 3), only a few decimetres below the sharp stratigraphic break at the base of the siliciclastic Wengen Formation. We do not exclude the possibility that similar ash layers also occur at stratigraphically higher levels, but their identification inside the clastic Wengen succession is challenging.

The stratigraphic positions of two of the three horizons with high-precision U–Pb zircon ages at Seceda (samples SEC-B; SEC-E

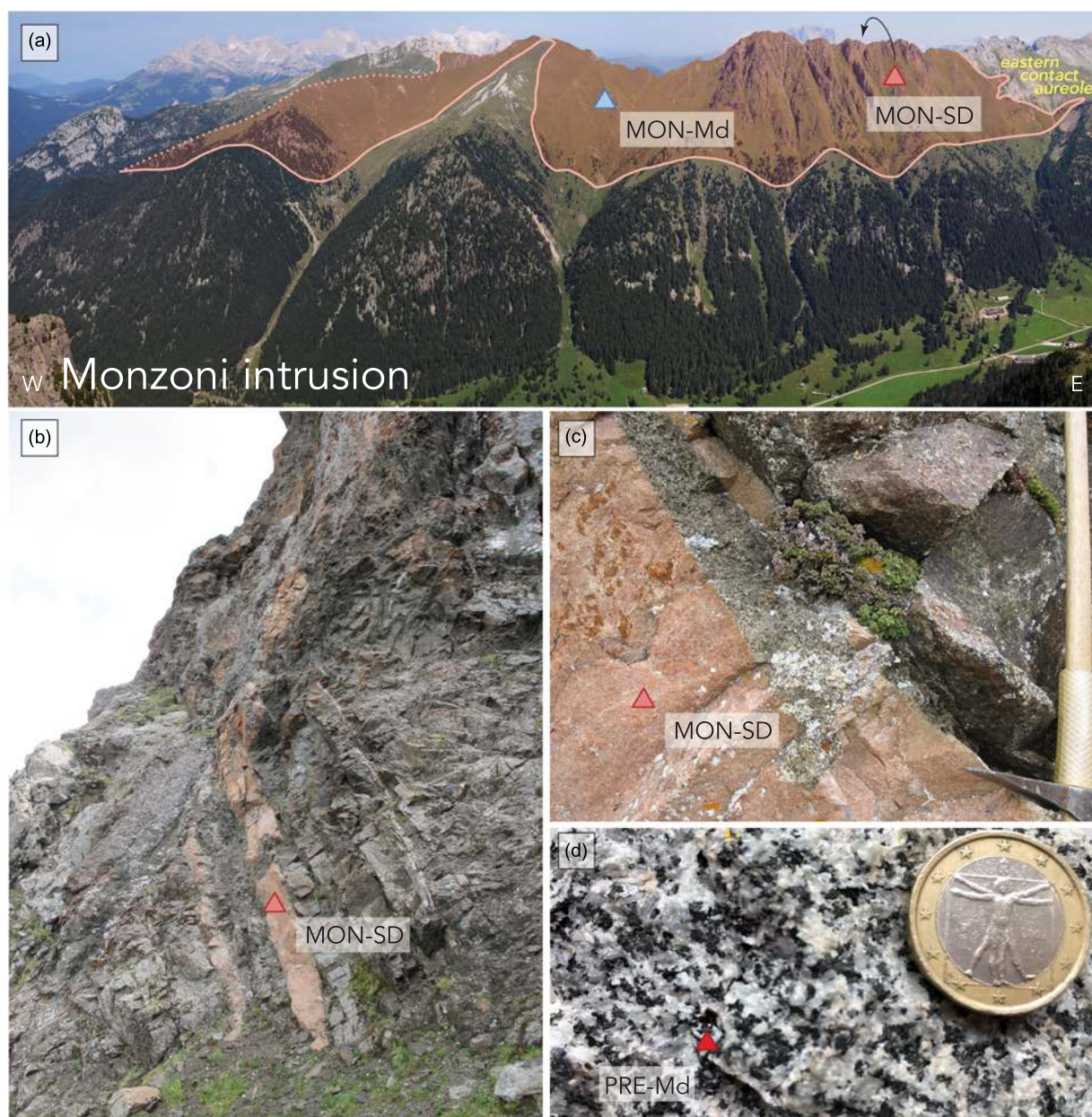


Fig. 5. (a) Panoramic view of the roughly SE–NW elongated southern slope of the Monzoni intrusion and its eastern margin forming a contact aureole in sediments including the Ladinian platform carbonates of the Costabella range. (b) Overview image and (c) detailed view of the syenite dyke injected into cumulitic pyroxenites at the eastern Monzoni intrusion. Blue and pale red triangles represent the actual sample localities of the dated monzodiorite (MON-Md) and syenite dyke (MON-SD). (d) Hand specimen of the dated monzodiorite (red triangle, PRE-Md) of the Predazzo intrusion (not illustrated here).

and SEC-G of Wotzlaw *et al.* 2018) can also be identified with confidence at Bagolino (Fig. 2). SEC-B is from a 1 cm thick crystal tuff at the base of the Tc-tuff interval. The same crystal tuff also occurs in the Lower Pietra Verde at Bagolino. Sample SEC-E is from a layer with accretionary lapilli (the LA-layer in Fig. 2). This lapilli layer can be identified in numerous sections in the Dolomites. At Bagolino, it occurs at the same stratigraphic position in the Middle Pietra Verde. The third sample at Seceda (SEC-G) is from an interval with carbonate turbidites and breccias in the upper part of the section immediately below layers with *Daonella tyrolensis* and *D. pichleri*. At Bagolino, this horizon probably corresponds to one of the layers in the Upper Pietra Verde – that is, below the beds with the same *Daonella* species in eastern Lombardy and Giudicarie. We presume that it could match a prominent coarse Pietra Verde layer at the 86 m level of the Bagolino column (Fig. 2).

Ash layers in successions of the northwestern Dolomites

Seceda–Pufels–Frötschbach

The stratigraphic successions of the Buchenstein Formation beneath Seiser Alm in the northwestern Dolomites are almost identical with the nearby section at Seceda (Fig. 2). In the lower two-thirds of the Buchenstein succession, volcanoclastic layers and individual basinal carbonate beds can be traced from Seceda to Pufels and Frötschbach (Brack & Rieber 1993; Brack & Muttoni 2000). The level corresponding to the Ladinian GSSP at Bagolino has been identified in all these sections (Wotzlaw *et al.* 2018).

The onset of mafic eruptions in the Seceda area is marked by pillow basalts at Mastlè Alm and west of the Kuka saddle at a stratigraphic level that can be pinpointed in the continuous volcanic-free reference Seceda section (Fig. 2). At Pufels, the base of a several hundred metre thick pile of extrusive and shallow intrusive



Fig. 6. Left-hand panel: pillow basalts of the mafic interval cropping out along a path near Kuka saddle south of Seceda. Right-hand panel: columnar basalt flow (Fernazza Formation) along the Frötschbach track close to Seiser Alm.

basalts lies at about the same stratigraphic level – that is, only a few metres above layers with *Daonella taramellii* in the uppermost Buchenstein Formation. At Frötschbach, the turbiditic upper Buchenstein Formation is replaced by clinoform breccias of the outermost Schlern carbonate platform slope. Higher up, the thick pile of volcanic rocks onlaps this slope and gradually pinches out towards the Schlern platform (Brandner *et al.* 2007).

Seiser Alm and Grohmann section

The thick pile of basalts at Seiser Alm is covered by a discontinuous interval of turbidites containing large amounts of reworked mafic volcanic material. The lower part of these sediments covers the presumably irregular top surface of the underlying basalt stack (Brandner *et al.* 2007). Mietto *et al.* (2012) named these sediments the ‘Frommer Member’ of the Fernazza Formation, whereas Brandner *et al.* (2007) merged it with the lithologically similar Wengen Formation. Along Frommerbach, the lowermost few metres of the turbiditic beds above the basalt top also consist of coarse Pietra Verde-like sandstone layers. Higher up, Wierer (1997) mentions several ash layers. A short survey of the Frommerbach section indeed revealed the presence of more than ten centimetre- to decimetre-thick whitish bentonite layers between 17 and 30 m above the top of the pillow basalt (see Fig. S5, Supplementary Material). However, none of the samples taken produced zircon crystals suitable for dating.

In the Tschapitbach section further south, only a single bentonite layer was found in the turbiditic sediments following on top of the pillow basalts (see also Mietto *et al.* 2012). However, the deposition of coarse conglomerates (the Marmolada conglomerate) may have removed part of the bentonite-bearing interval in this section. More bentonite layers again occur along an unnamed southern tributary of Frötschbach, immediately opposite Tschapitbach. In this section, the turbiditic sediments on top of the basalts reach *c.* 32 m in thickness. They are capped by massive clinoform breccia of the prograding upper part of the Schlern platform. The clastic interval hosts several centimetre- to decimetre-thick bentonites, which are most evident in the upper part (see Fig. S5, Supplementary Material). We assume that this section corresponds to ‘Rio Nigra’ in Mietto *et al.* (2012), from where these researchers report a precise U–Pb–zircon age. No exact location was given for

‘Rio Nigra’, but the locality is indicated in their topographic sketch in a creek *c.* 400 m further NW. However, the outcrops in that creek do not match the log in Mietto *et al.* (2012) and we could not find any ash layers there.

The stratigraphically highest samples analysed in this study are from the classic Grohmann section in the slopes south of Punta Grohmann, *c.* 10 km ESE of Seiser Alm. The summary section shown in Figure 2 largely follows the logs reported in Russo *et al.* (1997) and Gianolla *et al.* (1998). In the Grohmann section, coarse conglomerates of the Marmolada conglomerate follow directly on top of pillow breccias and hyaloclastites. No stratigraphic interval containing bentonites such as those at Seiser Alm is present in this section. This is either due to non-deposition on the irregular top surface of the volcanic rocks, or because such layers were removed during the deposition of the coarse conglomerates. The turbidite succession of the Wengen to Cassian formations also bears numerous layers with redeposited large carbonate blocks and spectacular slumped intervals. A set of two bentonites occurs stratigraphically *c.* 220 m above the top of the Marmolada conglomerate in this thick clastic succession. Samples PG-A and PG-B were taken from two centimetre-scale ash beds separated by *c.* 15 cm of marl (Fig. 4). We could not find any similar ash layers upwards from here to the top of the section.

Intrusive complexes of Predazzo and Monzoni

The Monzoni-Predazzo intrusive complex comprises the main intrusive bodies in the central/western Dolomites. The area around the Mt Monzoni complex is well known as the type locality of monzonite (De Lapparent 1864). It is composed of clinoproxenites, gabbros, monzogabbros, olivine gabbros, monzonites and a number of quartz syenitic and shoshonitic basaltic dykes cutting through adjacent Triassic sedimentary rocks and the intrusive massif (Bonadiman *et al.* 1994). We selected intermediate to more evolved monzodiorites from the Monzoni (MON-Md) intrusion (Fig. 5) and from the Predazzo Complex (PRE-Md). These lithologies form major intrusive units. A cross-cutting, late-stage syenite dyke (Fig. 5) from the Monzoni area (MON-SD) was selected to help constrain the duration of the igneous activity in this particular area.

Methods

U–Pb geochronology

Selected igneous zircons were dated using isotope dilution thermal ionization mass spectrometry (ID-TIMS) U–Pb geochronology after pre-screening larger populations using laser ablation inductively coupled plasma mass spectrometry. Zircons from seven samples – including four ash beds from Bagolino and Punta Grohmann, two monzodiorites from Predazzo and Monzoni and one syenite dyke from Monzoni – were separated using standard mineral separation techniques. Hand-picked zircons were annealed for 48 h at 900°C and then mounted in one-inch epoxy mounts and polished down to half the crystal thickness. Polished crystal interiors were imaged using a scanning electron microscope equipped with a cathodoluminescence detector. Subsequently, cathodoluminescence-imaged zircons were analysed for their trace element content and U/Pb isotope ratios by laser ablation inductively coupled plasma mass spectrometry using a Resonetics ArF excimer laser ablation system coupled with a Thermo ELEMENT XR sector field inductively coupled plasma mass spectrometer (Guillong *et al.* 2014). The Ti concentrations in zircon were determined relative to an updated Ti concentration of $4.73 \pm 0.15 \mu\text{g g}^{-1}$ for standard zircon 91500 (Szymanowski *et al.* 2018). Based on this pre-screening method, 45 zircons were selected for high-precision U–Pb geochronology applying chemical abrasion ID-TIMS techniques at the Institute of Geochemistry and Petrology at ETH Zurich (von Quadt *et al.* 2016; Wotzlaw *et al.* 2017). Pre-selected zircon grains were extracted from their epoxy mount using stainless-steel tools, transferred into 3 mL Savillex beakers and washed in 4 M HNO₃ in an ultrasonic bath. Cleaned zircon grains were loaded into 200 μL Savillex microcapsules for chemical abrasion (*c.* 13 h at 180°C; Mattinson 2005). Chemically abraded crystal fragments were transferred back into 3 mL Savillex beakers, fluxed in 6 M HCl at 110°C for several hours and ultrasonically cleaned three times in 4 M HNO₃. The zircon grains were transferred into their respective microcapsules, spiked with 5–10 mg of EARTHTIME ²⁰²Pb–²⁰⁵Pb–²³³U–²³⁵U tracer solution (ET2535; Condon *et al.* 2015; McLean *et al.* 2015) and dissolved in concentrated HF + trace HNO₃ for 60 h at 210°C in Parr bombs. The dissolved samples were dried and redissolved in 3 M HCl followed by ion-exchange chromatography (method modified from Krogh 1973). U–Pb separates were dried with a drop of 0.02 M H₃PO₄ and loaded onto outgassed Re filaments with *c.* 1 μL of Si-Gel emitter (method modified from Gerstenberger & Haase 1997). U and Pb isotope ratios were measured on a Thermo TRITON plus thermal ionization mass spectrometer using the protocols described in detail by Wotzlaw *et al.* (2018). The analytical results are reported in the Supplementary Material, Tables S1 and S2.

Age modelling

The high-resolution stratigraphic framework and zircon U–Pb geochronology dataset from this study, together with the consistent dataset of Wotzlaw *et al.* (2018), provides input for an extended age model of the Buchenstein Formation projected from the Seceda section towards the GSSP section at Bagolino (Figs 7–9). We used Bayesian age modelling applying the BACON age–depth modelling software of Blaauw & Christen (2011). The resulting continuous age–depth model provides age and uncertainty estimates (95% confidence envelope) for each layer (including non-dated ash layers) in the stratigraphic column (Fig. 9).

Results

ID-TIMS U–Pb geochronology

After correction for ²³⁰Th disequilibrium, the majority of analysed ash bed zircons yielded concordant ²⁰⁶Pb/²³⁸U and ²⁰⁷Pb/²³⁵U

dates. Minor residual discordance can be accounted for by inaccuracies in the ²³⁵U decay constant (Schoene *et al.* 2006; Mattinson 2010), initial ²³¹Pa disequilibrium (Schmitt 2007; Rioux *et al.* 2015) and U isotopic heterogeneities (Hiess *et al.* 2012) or a combination of these factors. None of these factors significantly affects the ²⁰⁶Pb/²³⁸U dates that we take as the crystallization age of each zircon. However, interpreting eruption and ash bed deposition ages from zircon U–Pb dates has been a matter of intense debate because zircon crystallization may significantly predate eruption (Simon *et al.* 2008; Wotzlaw *et al.* 2014). We therefore provide different age interpretations of ash bed depositional ages as well as the emplacement and crystallization ages for the intrusions in Table 1. These interpretations are based on: (1) the ²³⁰Th-corrected ²⁰⁶Pb/²³⁸U date of the youngest dated closed-system zircon; (2) the weighted mean of the youngest population of statistically equivalent ²³⁰Th-corrected ²⁰⁶Pb/²³⁸U dates of a sample; and (3) a Bayesian eruption age estimate using the approach of Keller *et al.* (2018). For consistency with the data published by Wotzlaw *et al.* (2018), the following results and related age interpretations are based on the weighted mean dates as our preferred estimate for the deposition ages of dated ash beds and the emplacement ages of the intrusions (Fig. 7).

Eight zircons were analysed from sample BG-CG with uncertainties on single zircons between 0.068 and 0.114 Ma. Five zircons yielded statistically equivalent dates with a weighted mean ²⁰⁶Pb/²³⁸U date of 242.653 ± 0.036 Ma (MSWD = 0.5). Two zircons yielded significantly younger dates and are interpreted to be affected by residual Pb loss despite the chemical abrasion pre-treatment. One zircon yielded an older date of 243.109 ± 0.068 Ma.

Eight analyses from sample BG-92.2 yielded a more complex distribution of ²⁰⁶Pb/²³⁸U dates with a bimodal distribution. Four zircons yielded statistically equivalent dates with a weighted mean ²⁰⁶Pb/²³⁸U date of 238.646 ± 0.037 Ma (MSWD = 0.7). The older populations of zircons are interpreted to be recycled antecrysts.

Four zircons were analysed from each of the two bentonites in the Grohmann section. ²⁰⁶Pb/²³⁸U dates of zircons from the upper layer PG-B are statistically equivalent with a weighted mean of 237.579 ± 0.042 Ma (MSWD = 2.8). Three of four zircons analysed from PG-A yielded equivalent ²⁰⁶Pb/²³⁸U dates with a weighted mean of 237.680 ± 0.047 Ma (MSWD = 0.5). These two dates are distinguishable at the 95% confidence level and are in stratigraphic order. The single-grain dates of the two ash beds are indistinguishable.

Between six and eight zircons were analysed from each of the three samples from the Monzoni-Predazzo intrusive complex (PRE-Md, MON-Md and MON-SD). ²³⁰Th-corrected ²⁰⁶Pb/²³⁸U dates range from 238.190 ± 0.050 to 238.075 ± 0.087 Ma. Five of seven zircons from MON-Md yielded a weighted mean ²⁰⁶Pb/²³⁸U date of 238.190 ± 0.050 Ma (MSWD = 0.9) and five of six zircons from the syenite dyke MON-SD yielded an indistinguishable weighted mean of 238.137 ± 0.050 Ma (MSWD = 1.1). Despite being statistically equivalent, the younger date for MON-SD is consistent with cross-cutting relationships (Fig. 5). Five of eight zircons from the monzodiorite of Predazzo (PRE-Md) yielded a weighted mean ²⁰⁶Pb/²³⁸U date of 238.075 ± 0.087 Ma (MSWD = 2.2), therefore representing the youngest intrusive unit dated in this study.

Age–depth modelling of the volcano-sedimentary sequence at Bagolino

Age–depth models allow the derivation of robust age estimates for stratigraphic levels that were not directly dated. Using the BACON age–depth modelling software (Blaauw & Christen 2011), we constructed age–depth models for the volcano-sedimentary sequence at Bagolino. We tested the sensitivity of the models

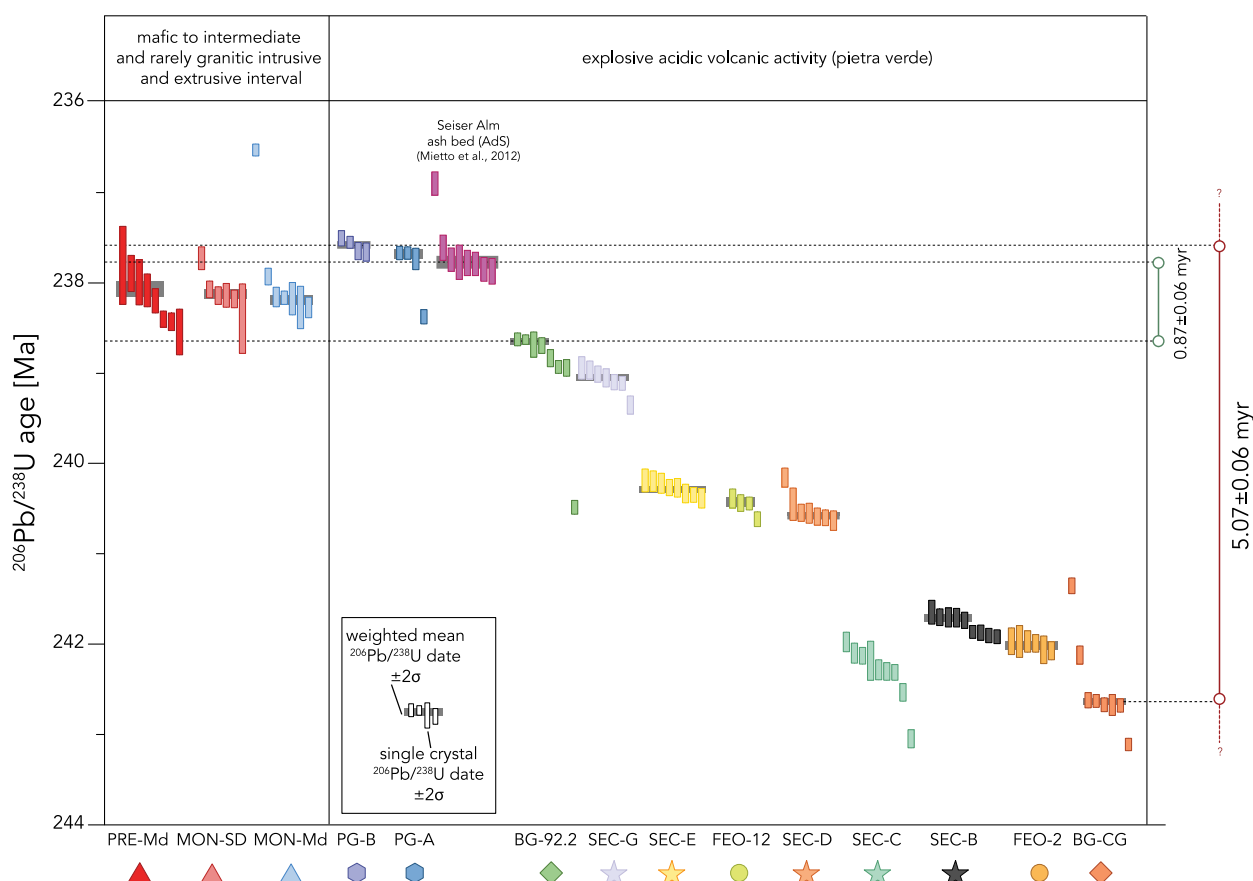


Fig. 7. $^{206}\text{Pb}/^{238}\text{U}$ isotope age systematics of analysed single crystals (vertical bars) from volcanic ash beds (right-hand side) and intermediate composition intrusive bodies in the Dolomites (left-hand side). Grey horizontal bars indicate weighted mean ages for dated samples. Dated samples from this study (BG-CG, BG-92.2, PG-A, PG-B, PRE-Md, MON-Md, MON-SD) are complemented by the dataset of [Wotzlaw *et al.* \(2018\)](#) (FEO-2, FEO-12, SEC-B, SEC-C, SEC-D, SEC-E and SEC-G). BG-CG to PG-B constrain a duration of the magmatic interval to at least 5.07 ± 0.06 myr. BG-92.2 and AdS bracket the duration of the mafic extrusive interval to 0.87 ± 0.06 myr.

depending on the different age interpretations for ash bed deposition (Table 1; Figs 8 and 9). Figure 8 shows how the different age interpretations affect the age–depth model results at Bagolino. All three approaches yield almost linear sediment accumulation rates over the entire range. Larger uncertainties on the input data derived from the youngest zircon and Bayesian eruption age estimates yield wider 95% confidence interval envelopes. As a result of the stable sedimentary environment and constant sedimentation rate, the different age interpretations do not significantly affect the shape of the age–depth model, but result in a systematic shift. This systematic shift results in slightly different model ages for the Ladinian GSSP level (Fig. 9). Such differences resulting from different zircon age interpretation approaches should be taken into account in future calibrations of the geological timescale. For consistency and comparison with the precursor study of [Wotzlaw *et al.* \(2018\)](#), the age–depth model shown in Figure 9 uses the weighted mean dates of each ash bed as the model input. This age model provides additional age constraints for undated volcanic products within the stratigraphic sequence.

Zircon trace element geochemistry

The trace element compositions of zircons show distinct geochemical signatures for the intrusions, the ash beds erupted before the mafic interval and the ash beds erupted after the mafic interval (Fig. 10). Bivariate diagrams of Th/U v. Ce/Nd and Yb/Dy (Fig. 10) clearly discriminate these three compositional groups. Zircons from both ash beds and intrusions show consistent core–rim compositional relationships (Fig. 10). Most crystals display decreasing

Th/U ratios with increasing Ce/Nd and Yb/Dy ratios as well as a more pronounced negative Eu anomaly from core to rim (Eu/Eu^* , not illustrated). These geochemical characteristics are consistent with the progressive crystallization of zircon together with amphibole \pm titanite and plagioclase \pm K-feldspar from an evolving melt ([Wotzlaw *et al.* 2013](#); [Samperton *et al.* 2015](#); [Large *et al.* 2018](#)).

Ti-in-zircon thermometry

The Ti concentrations in zircon range from 1.1 to 22.5 ppm for the ash beds, with decreasing Ti contents from core to rim consistent with progressive cooling (Fig. 11). The intrusions of Predazzo and Monzoni show Ti concentrations between 1.6 and 17.2 ppm, with less pronounced core–rim concentration gradients towards lower Ti concentrations in the rims. Both monzodiorite samples show equivalent trends, whereas zircons from the late-stage quartz syenite dyke record lower Ti concentrations. Zircon crystallization temperatures based on the calibration of the Ti-in-zircon thermometer of [Ferry & Watson \(2007\)](#) have been calculated assuming $a_{\text{TiO}_2} = 0.7$ and $a_{\text{SiO}_2} = 1$ for all samples. Monzodiorite zircons yielded crystallization temperatures between 725 and 830°C. Zircons from the quartz syenitic dyke of Monzoni record lower crystallization temperatures (660–770°C). The calculated Ti-in-zircon temperatures for ash bed zircons show a large temperature range of $>200^\circ\text{C}$ (650 to $>850^\circ\text{C}$), with higher temperatures for core analyses. The zircon rims cluster in a narrow temperature window between 650 and 720°C, close to the granitic solidus, with only a few rim analyses resulting in higher temperatures.

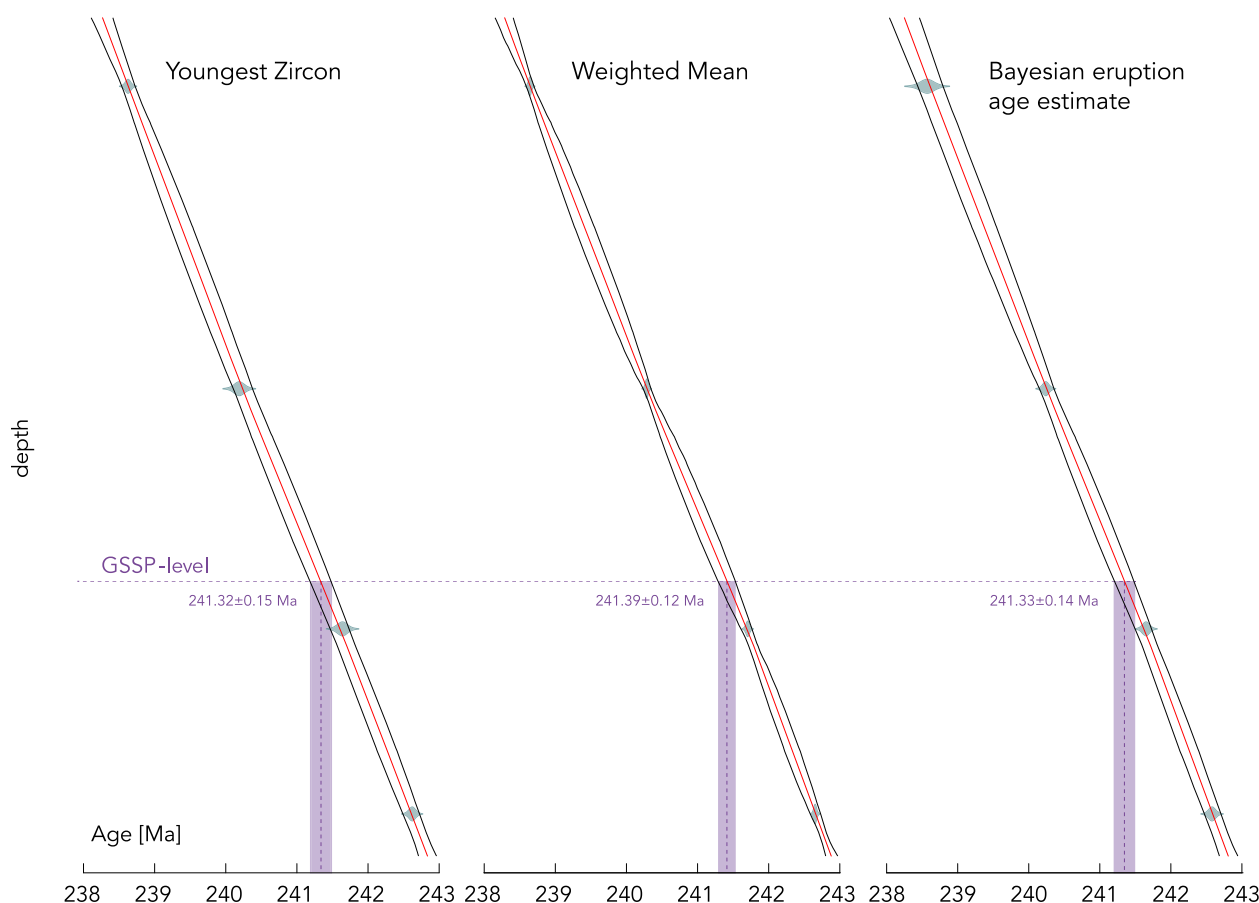


Fig. 8. Comparison of Bayesian age–depth model approach considering three different age interpretation approaches (youngest zircon age, weighted mean and Bayesian eruption age estimate) for the samples (BG-CG, SEC-B, SEC-E and BG-92.2) in Table 1. Vertical purple bars indicate different numerical estimates for the Anisian–Ladinian Global Boundary Stratotype Section and Point level.

U/Yb and Nb/Yb systematics

The trace element composition of igneous zircons strongly depends on the composition of the parental melt. Grimes *et al.* (2015) introduced a discrimination scheme relating the composition of igneous zircon to the geotectonic environment. Zircons from oceanic islands, mid-ocean ridges and continental arc-type settings can be distinguished on a bivariate diagram of $\log(U/Yb)$ v. $\log(Nb/Yb)$ (Fig. 12). Schmitt *et al.* (2017) extended this scheme to rear-arc settings. The zircons from both the Middle Triassic intrusions and volcanic rocks plot above and sub-parallel to the mantle array well within the pre-defined continental arc-type field.

Discussion

Duration of Anisian–Ladinian magmatism in the Southern Alps

The duration of magmatic activity can be constrained by the oldest and youngest dated magmatic products. The oldest dated product is a volcanic ash bed from the Contrada Gobbia interval of the Bagolino section (sample BG-CG; Fig. 7) dated at 242.653 ± 0.036 Ma. The youngest dated product is an ash bed just below the upper Ladinian to Lower Carnian boundary from the Punta Grohmann section dated at 237.579 ± 0.042 Ma. Stratigraphically, this level is younger than an ash bed from a section at Seiser Alm dated at 237.773 ± 0.052 Ma (Mietto *et al.* 2012). These ash beds constrain the duration of Middle Triassic magmatism to at least 5.07 ± 0.06 myr. As these ash beds are also stratigraphically constrained to be the oldest and youngest products within the stratigraphic interval investigated in this study, we are confident

that this duration is not significantly underestimated due to under-sampling (e.g. Glazner & Sadler 2016).

Duration of basaltic effusive magmatism

The duration of basaltic effusive magmatism can be constrained by bracketing the zircon-bearing volcanic ash beds that can be dated using the U–Pb technique. The youngest volcanic ash bed sampled at Bagolino and dated at 238.646 ± 0.037 Ma and the ash bed from Seiser Alm dated at 237.773 ± 0.052 Ma reported by Mietto *et al.* (2012) bracket the main interval of basaltic lavas. This constrains the main phase of basaltic eruptions to a short interval of $<0.87 \pm 0.06$ myr.

Age of intrusive complexes and relationship with basaltic lava flows

The zircon U–Pb dates of the monzonitic intrusions and the syenitic dyke from Predazzo and Monzoni point towards a protracted emplacement between 238.190 ± 0.050 and 238.075 ± 0.087 Ma. However, due to the short time interval covered by these intrusive units, they are combined into a single system. The dated intrusive units are age-equivalent to the basaltic lava flows bracketed by ash beds from the Seceda and Punta Grohman sections. Therefore we interpret the subvolcanic rocks of Monzoni–Predazzo as part of a feeder system directly linked to the basaltic lavas.

Magmatic processes

We did not observe any indication of a continuously evolving single upper crustal magmatic reservoir governing the trace element record

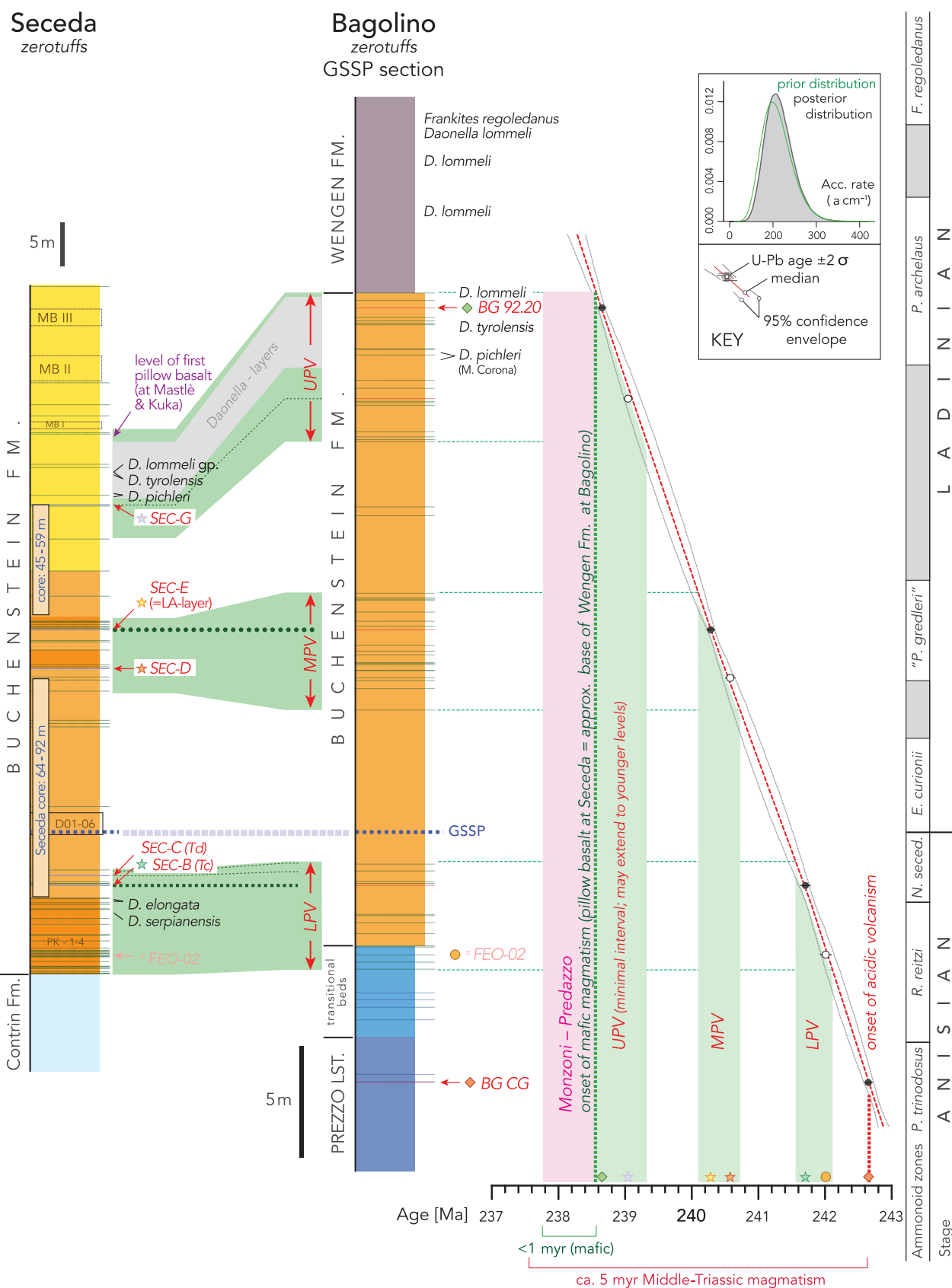


Fig. 9. Bayesian age model for the Middle Triassic magmatic interval calculated for the Global Boundary Stratotype Section and Point reference section at Bagolino. Left-hand panel shows the correlation of the Seceda and Bagolino sections with marked positions of the dated volcaniclastic layers within the Lower, Middle and Upper Pietra Verde (LPV, MPV and UPV) intervals; stratigraphic correlation of the intrusive complexes of Predazzo and Monzoni are based on isotope dilution thermal ionization mass spectrometry ages, cross-cutting relationships and their relative position in the stratigraphic column. The Bayesian age model was constructed using the new U-Pb dates for Bagolino along with two values from Seceda (SEC-B, SEC-E) for layers that can be unambiguously correlated to Bagolino. Green bars highlight the three main intervals of Pietra Verde concentrations. The red bar denotes the maximum interval for the main pulse of mafic volcanism in the Dolomites. Symbols refer to the studied ash layers shown in Figures 7, 10 and 11.

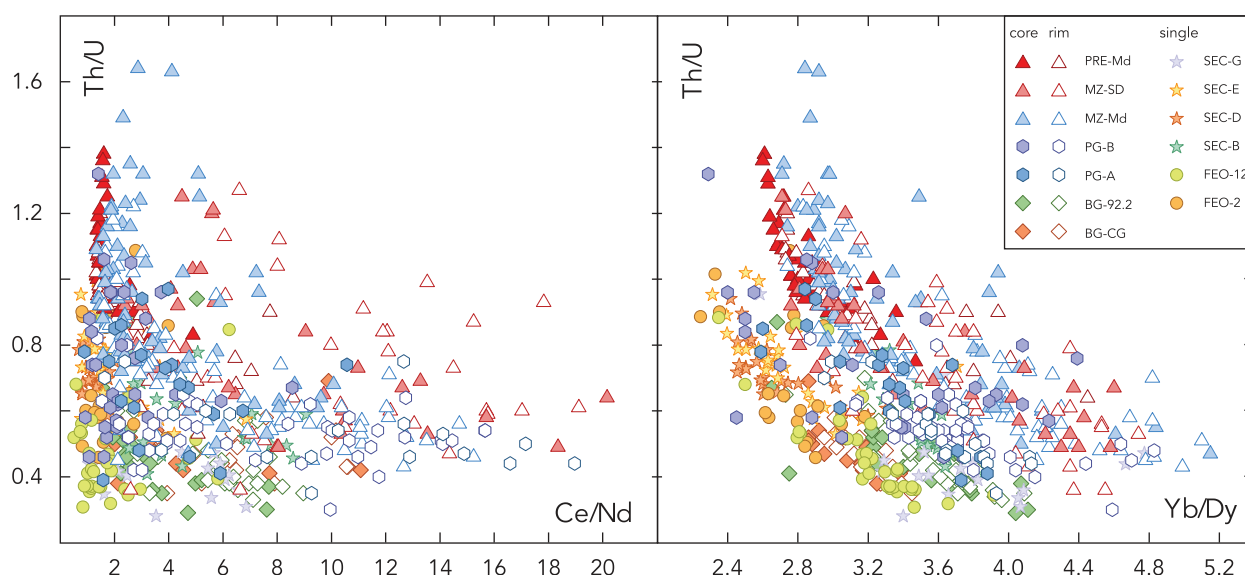


Fig. 10. Binary trace element variation diagrams of zircons from volcanic ash beds at Bagolino, Passo Feudo, Seceda and the Monzoni-Predazzo intrusive complex. Symbols and colour codes are the same as in Figure 7. Cores and rims are indicated by closed and open symbols with identical colour codes, respectively. Trace element data obtained by single laser ablation inductively coupled plasma mass spectrometry spot analysis; data for samples FEO-2, FEO-12, SEC-B, SEC-D, SEC-E and SEC-G are from Wotzlaw *et al.* (2018).

of the magmatic zircons from older to younger samples for either the ash beds or the intrusive rocks. Nevertheless, some of the within-sample core to rim relationships can be explained by fractional crystallization processes.

This seemingly discontinuous record for the volcanic ash beds supports the hypothesis of independently evolving geographically dispersed upper crustal magmatic bodies and their respective volcanic centres forming several irregularly distributed vents

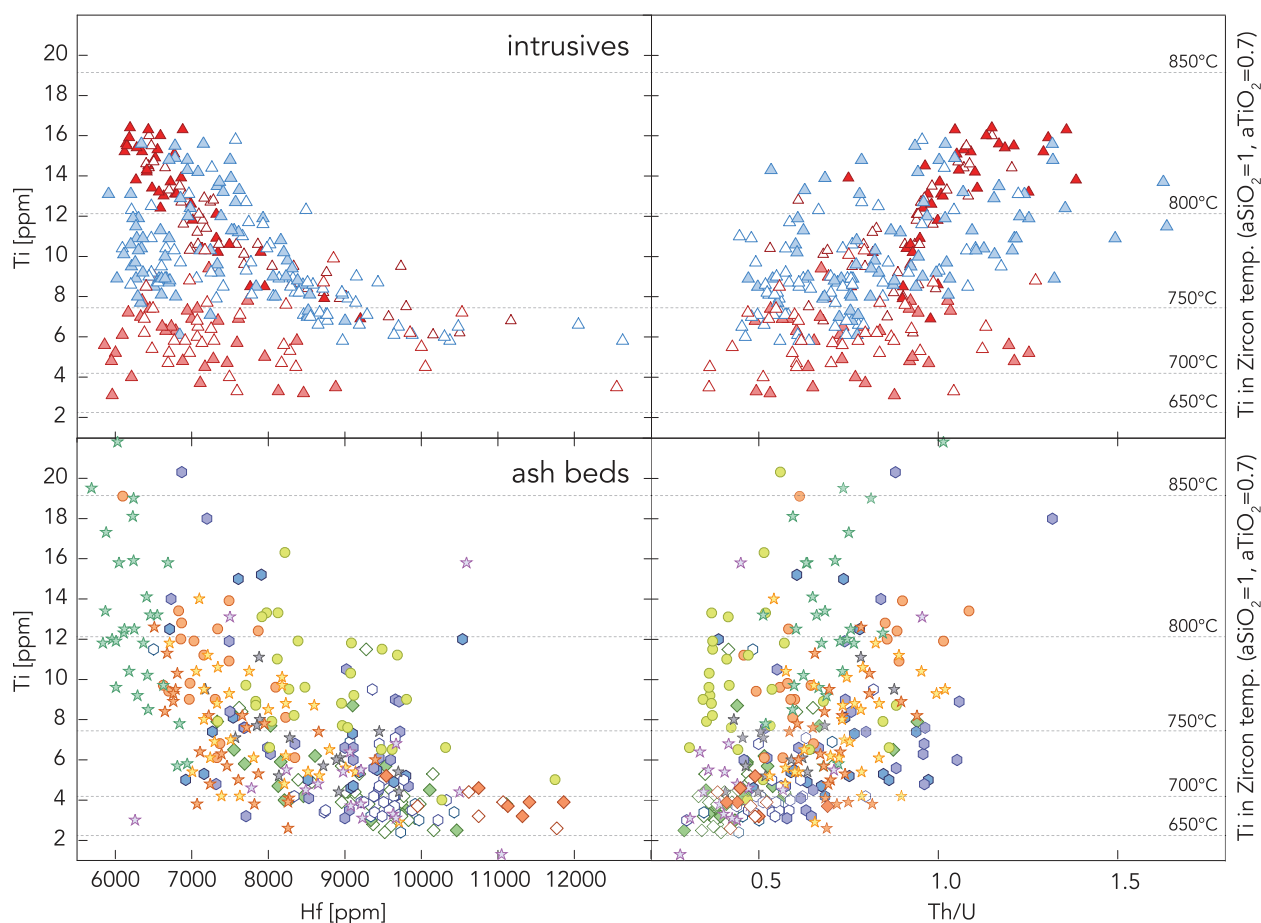


Fig. 11. Ti v. Th/U and Hf concentration diagrams with Ti-in-zircon temperatures based on Ferry & Watson (2007). Symbols and colour codes are the same as in Figure 7.

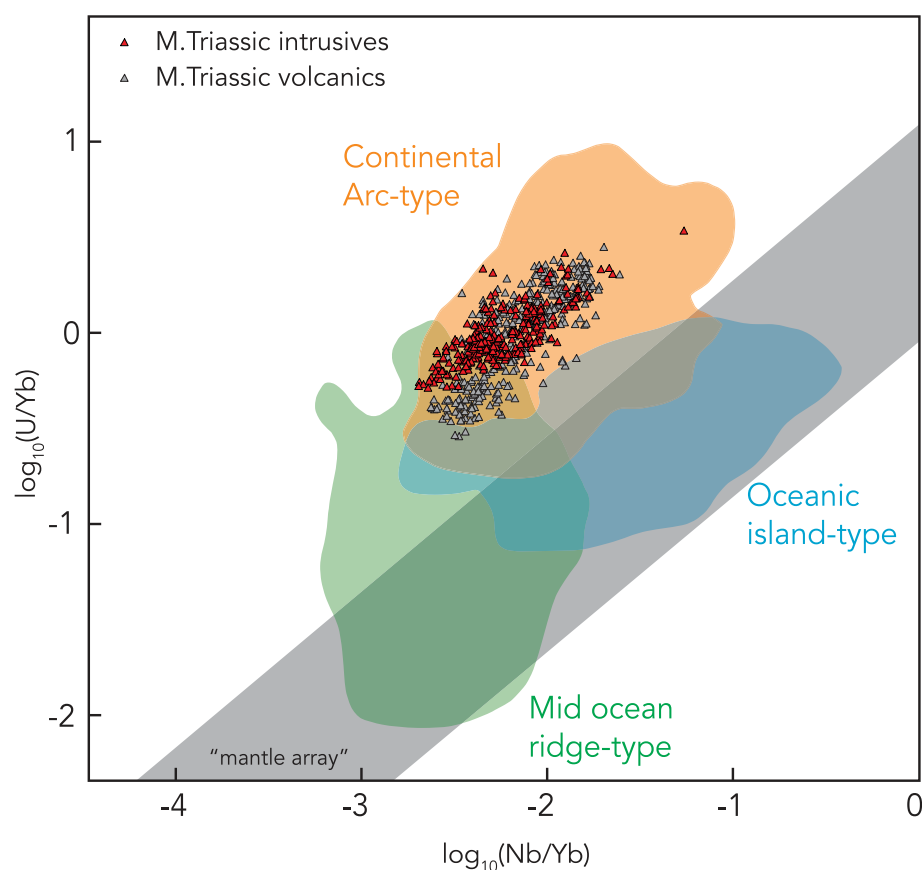


Fig. 12. Bivariate diagram of $\log(U/Yb)$ v. $\log(Nb/Yb)$ for zircon trace elements modified after the defined and compiled zircon trace element datasets of Grimes *et al.* (2015) used as a discrimination scheme relating the composition of igneous zircon to geotectonic settings (oceanic islands, mid-ocean ridges and continental arc-type settings). The shaded fields are overlapping two-dimensional kernel density distributions with contours shown for 95% confidence levels. The 'mantle-zircon array' after Grimes *et al.* (2015) is indicated in grey.

throughout the Southern Alpine realm. Similar geochemical characteristics for ash beds with different ages, such as BG-92.2 and SEC-G (e.g. Yb/Dy v. Th/U , Fig. 10), may indicate common source magmas. We speculate that the previously introduced (sub) volcanic bodies of rhyolitic–rhyodacitic composition of the Tarvisio area (Spadea 1970) and Recoaro (De Vecchi & Sedeà 1983) possibly represent such isolated upper crustal bodies sourcing the Pietra Verde volcanism in the Southern Alps.

Spatio-temporal distribution and correlation of intrusive and volcanic products in the Southern Alps

Single-grain ID-TIMS ages for the volcanoclastic ash beds show that the younger intrusive bodies in the Dolomites are not the source of the Pietra Verde ash layers. Other potential sources in eastern Lombardy (Muffetto), Recoaro and Tarvisio are still not confirmed. The transitional trace element characteristics (e.g. Yb/Dy v. Th/U , Fig. 10) of the younger ash layers from Punta Grohmann are consistent with an intermediate source character, such as at Predazzo and Monzoni. The lack of zircons in ash beds at Seiser Alm (Figs 1 and 2) indicate the more mafic character of these ash beds and therefore their affiliation with the late-stage magmatic bodies in the Dolomites that may have acted as their source.

The spatio-temporal distribution of potential volcanic vents for the Pietra Verde layers has not yet been unravelled. With our high-resolution petrochronological framework, further stratigraphically unconstrained volcanic products – such as the volcanoclastic rocks and shallow intrusions of the Recoaro and Tarvisio areas and beyond – may be linked with the ash beds dated in this study by either U–Pb geochronology and/or their trace element fingerprint.

Geodynamic scenario

Most previously discussed speculations and interpretations addressing the geodynamic scenario of the Middle Triassic magmatic

system are based on whole-rock geochemical data, including the intrusive bodies at Predazzo and Monzoni, and field observations. Several scenarios have been proposed to explain the geochemical character (the relative Nb–Ta and Ti depletion related to mobile phases derived from subducted oceanic lithosphere containing retentive phases such as rutile and titanite) of the Middle Triassic shoshonite magmatism. Summarized by Pisa *et al.* (1980), these include: (1) extensional processes with fracturing of the crust predating the Jurassic opening of the central Tethys; (2) increased heat flow underneath a crust thickened during the Variscan Orogeny; (3) the Middle Triassic collapse of a Variscan orogenic nucleus with magmatism linked to a late Variscan tectonic event; and (4) active subduction processes.

Castellarin *et al.* (1988) envisaged lithospheric foundering linked to the subduction of the Palaeotethys Ocean further east. In a similar model, Cassinis *et al.* (2008) considered the Middle Triassic magmatism as an expression of an arc/back-arc setting characterized by trans-tensional tectonic conditions related to subduction at the eastern margin of palaeo-Europe. The limited isotopic–geochemical data available for the Monzoni intrusion show low initial $^{87}Sr/^{86}Sr$ ratios between 0.7041 and 0.7047 and ϵNd values between -0.34 and -2.60 (Masch & Huckenholz 1993). Masch & Huckenholz (1993) suggested that a radiogenically enriched upper mantle reservoir contaminated with old, mafic lower crust sourced the shallow level Monzoni intrusion in the Dolomites. The trace element composition of zircons analysed in this study suggest a continental arc affinity (Fig. 12; Grimes *et al.* 2015), which is in agreement with the studies of Castellarin *et al.* (1988) and Cassinis *et al.* (2008) and the existence of a metasomatized subcontinental lithospheric mantle reservoir. However, this does not conclusively prove the existence of a subduction-related process. Continental arc-type patterns could also be the result of the foundering of lower crustal igneous cumulates from Variscan and/or Permian magmatic events and partial melting of the same together with mantle melting, similar to the process described for the Chilas Komplex in Kohistan

Table 1. Summary of U–Pb geochronology results for ash beds and intrusions from Bagolino, Punta Grohmann, Predazzo and Monzoni.

| Sample | Stratigraphic position at Bagolino (m)* | Youngest $^{206}\text{Pb}/^{238}\text{U}$ date (Ma) | 95% CI ‡ , X/Y/Z (Ma) | Weighted mean $^{206}\text{Pb}/^{238}\text{U}$ date (Ma) | 95% CI ‡ , X/Y/Z (Ma) | MSWD ‡ | Bayesian model date § (Ma) | 95% CI ‡ (Ma) |
|-------------------------|---|---|-----------------------------------|--|-----------------------------------|--------------------|----------------------------------|---------------------------|
| BG-CG | −8.83 | 242.621 | 0.083/0.17/0.31 | 242.653 | 0.036/0.12/0.29 | 0.50 | 242.581 | 0.092/0.12/0.29 |
| FEO-2 ^W | | 241.97 | 0.15/0.16/0.29 | 242.010 | 0.050/0.088/0.26 | 0.62 | 241.989 | 0.061/0.095/0.28 |
| SEC-B ^W | 0.00 | 241.64 | 0.13/0.15/0.28 | 241.705 | 0.045/0.093/0.29 | 0.34 | 241.647 | 0.091/12/0.29 |
| SEC-C ^W | | 241.98 | 0.11/0.13/0.27 | Out of stratigraphic order/no w. mean Bayesian eruption date estimate calculated | | | | |
| SEC-D ^W | | 240.45 | 0.18/0.19/0.31 | 240.576 | 0.042/0.084/0.25 | 0.81 | 240.563 | 0.054/0.090/0.28 |
| FEO-12 ^W | | 240.39 | 0.11/0.13/0.27 | 240.428 | 0.049/0.087/0.26 | 0.37 | 240.38 | 0.10/0.12/0.29 |
| SEC-E ^W | 11.46 | 240.19 | 0.13/0.15/0.28 | 240.285 | 0.036/0.081/0.25 | 1.90 | 240.239 | 0.084/0.11/0.29 |
| SEC-G ^W | | 238.94 | 0.12/0.14/0.28 | 239.044 | 0.038/0.081/0.25 | 2.10 | 238.941 | 0.091/0.12/0.29 |
| BG-92.2 | 25.89 | 238.626 | 0.069/0.14/0.29 | 238.643 | 0.037/0.11/0.28 | 0.77 | 238.57 | 0.18/0.19/0.33 |
| MON-Md | | 238.16 | 0.11/0.15/0.30 | 238.190 | 0.050/0.11/0.28 | 0.87 | 237.61 | 0.18/0.19/0.33 |
| MON-SD | | 238.078 | 0.091/0.14/0.29 | 238.137 | 0.050/0.13/0.29 | 1.10 | 237.515 | 0.083/0.11/0.28 |
| PRE-Md | | 237.81 | 0.43/0.44/0.51 | 238.075 | 0.087/0.15/0.29 | 2.20 | 237.91 | 0.15/0.17/0.31 |
| PG-A | | 237.670 | 0.075/0.16/0.30 | 237.680 | 0.047/0.13/0.28 | 0.50 | 238.124 | 0.061/0.094/0.28 |
| PG-B | | 237.509 | 0.084/0.15/0.30 | 237.579 | 0.042/0.12/0.28 | 2.79 | 237.81 | 0.28/0.29/0.39 |
| GSSP level ^M | 2.39 | 241.32 | 0.15/0.16/0.31 | 241.393 | 0.123/0.14/0.30 | | 241.33 | 0.14/0.16/0.31 |

*Stratigraphic positions refer to the Bagolino zero-tuff log.

†Uncertainties are given as 95% confidence intervals (CI) at three levels of uncertainty propagation: X is the analytical uncertainty; Y includes X and the tracer calibration uncertainty (Condon *et al.* 2015); Z includes X, Y and the ^{238}U decay constant uncertainty (Jaffey *et al.* 1971).

‡MSWD, mean square weighted deviation.

§Bayesian eruption age estimate after Keller *et al.* (2018).

¶Values for Anisian–Ladinian GSSP level at Bagolino zero-tuff log calculated with BACON Bayesian age modelling software after Blaauw & Christen (2011).

ⓂResults from Seceda and Passo Feudo are taken from Wotzlaw *et al.* (2018) with recalculated Bayesian eruption age estimates.

(Jagoutz *et al.* 2011; Jagoutz & Schmidt 2012, 2013; Müntener & Ulmer 2018). Potential magmatic processes include the peritectic melting of amphibole-rich cumulates serving as a supply of H_2O and retentive Ti oxide (rutile or ilmenite) restitic material. The breakdown of these amphibole-rich cumulates might be linked to a limited H_2O content of the magmas (2 wt.% H_2O) relative to typical (active arc) magmas, resulting in steeper K_2O v. SiO_2 curves (a shoshonitic trend), as proposed by Meen (1987) and Müntener & Ulmer (2018).

Conclusions

We have presented a geochronological framework for Middle Triassic intrusive and volcanic products from the Southern Alps. Our high-precision zircon U–Pb geochronology dataset, together with the high-resolution integrated stratigraphic framework, precisely constrain the timing and evolution of this magmatic interval. The main interval of Middle Triassic magmatism in the Southern Alps lasted at least 5.07 ± 0.06 myr. Early silicic eruptions between 242.653 ± 0.036 and 238.646 ± 0.037 Ma were followed by a short eruptive interval of voluminous basaltic lava flows bracketed by silicic tuffs to $<0.87 \pm 0.06$ myr. Mafic to intermediate intrusions of the Monzoni–Predazzo intrusive complex were dated at 238.190 ± 0.050 – 238.075 ± 0.087 Ma and are coeval with the mafic interval. The youngest products are tuffs from late Ladinian to early Carnian sequences dated at 237.680 ± 0.047 and 237.579 ± 0.042 Ma. This geochronological framework provides tight constraints on the timing and evolution of Middle Triassic magmatism in the Southern Alps.

Acknowledgements The authors thank M. Guillon and A. von Quadt for technical support, N. Preto and two anonymous reviewers for constructive comments and I.M. Villa for editorial handling.

Funding This study was funded by the Swiss National Science Foundation.

Scientific editing by Igor Villa

References

- Abbas, H., Michail, M., Cifelli, F., Mattei, M., Gianolla, P., Lustrino, M. & Carminati, E. 2018. Emplacement modes of the Ladinian plutonic rocks of the Dolomites: insights from anisotropy of magnetic susceptibility. *Journal of Structural Geology*, **113**, 42–61.
- Assereto, R., Jadoul, F. & Omenetto, P. 1977. Stratigrafia e metallogenesi del settore occidentale del distretto a Pb, Zn, fluorite e barite di Gorno (Alpi Bergamasche). *Rivista Italiana di Paleontologia e Stratigrafia*, **83**, 395–532.
- Balini, M. & Renesto, S.C. 2012. Cymbospondylus vertebrae (Ichthyosauria, Shastasauridae) from the Upper Anisian Prezzo Limestone (Middle Triassic, southern Alps) with an overview of the chronostratigraphic distribution of the group. *Rivista Italiana di Paleontologia e Stratigrafia*, **118**, 155–172.
- Bébien, J., Blanchet, R., Cadet, J.P., Charvet, J., Chorowicz, J., Lapiere, H. & Rampoux, J.P. 1978. Le volcanisme triasique des Dinarides en Yougoslavie: Sa place dans l'évolution géotectonique péri-méditerranéenne. *Tectonophysics*, **47**, 159–176.
- Berra, F. & Carminati, E. 2010. Subsidence history from a backstripping analysis of the Permo-Mesozoic succession of the Central Southern Alps (northern Italy). *Basin Research*, **22**, 952–975.
- Bertotti, G., Picotti, V., Bernoulli, D. & Castellarin, A. 1993. From rifting to drifting: tectonic evolution of the South-Alpine upper crust from the Triassic to the Early Cretaceous. *Sedimentary Geology*, **86**, 53–76.
- Blaauw, M. & Christen, J.A. 2011. Flexible paleoclimate age–depth models using an autoregressive gamma process. *Bayesian Analysis*, **6**, 457–474.
- Bonadiman, C., Coltorti, M. & Siena, F. 1994. Petrogenesis and T–fO₂ estimates of Mt Monzoni complex (Central Dolomites, Southern Alps): a Triassic shoshonitic intrusion in a transcurrent geodynamic setting. *European Journal of Mineralogy*, **6**, 943–966.
- Bosellini, A., Gianolla, P. & Stefani, M. 2003. Geology of the Dolomites. *Episodes*, **26**, 181–185.
- Brack, P. & Muttoni, G. 2000. High-resolution magnetostratigraphic and lithostratigraphic correlations in Middle Triassic pelagic carbonates from the Dolomites (northern Italy). *Palaeogeography, Palaeoclimatology, Palaeoecology*, **161**, 361–380.
- Brack, P. & Rieber, H. 1993. Towards a better definition of the Anisian/Ladinian boundary: new biostratigraphic data and correlations of boundary sections from the Southern Alps. *Eclogae Geologicae Helvetiae*, **86**, 415–527.
- Brack, P., Rieber, H., Nicora, A. & Mundil, R. 2005. The Global Boundary Stratotype Section and Point (GSSP) of the Ladinian Stage (Middle Triassic) at Bagolino (Southern Alps, northern Italy) and its implications for the Triassic time scale. *Episodes*, **28**, 233–244.
- Brack, P., Rieber, H., Mundil, R., Blendinger, W. & Maurer, F. 2007. Geometry and chronology of growth and drowning of Middle Triassic carbonate platforms (Cembra and Biviera/Clapsavon) in the Southern Alps (northern Italy). *Swiss Journal of Geosciences*, **100**, 327–348.
- Brandner, R., Burger, U. *et al.* 2007. *Geologische Karte der Westlichen Dolomiten, West-Blatt, Ost-Blatt und Profilschnitte*, 1:25.000. Autonome

- Provincia Bozen – Südtirol, Amt für Geologie und Baustoffprüfung. Litografia artistica Cartografica, Florence.
- Brasca, C., Gaetani, M., Jadoul, F. & Viel, G. 1981. Paleogeografia ladinico-carnica e metallogenesi del sudalpino. *Memorie della Società Geologica Italiana*, **22**, 65–82.
- Callegari, E. & Monese, A. 1964. Il chimismo della pietra verde degli Strati di Livinallongo (Dolomiti). Contributo allo studio petrogenetico della 'pietra verde' ladinica. *Studi Trentini di Scienze Naturali*, **41**, 45–71.
- Casetta, F., Coltorti, M. & Marrocchino, E. 2018. Petrological evolution of the Middle Triassic Predazzo Intrusive Complex, Italian Alps. *International Geology Review*, **60**, 977–997.
- Cassinis, G., Cortesogno, L., Gaggero, L., Perotti, C.R. & Buzzi, L. 2008. Permian to Triassic geodynamic and magmatic evolution of the Brescian Prealps (eastern Lombardy, Italy). *Bollettino della Società geologica italiana*, **127**, 501–518.
- Castellarin, A., Lucchini, F., Rossi, P., Selli, L. & Simboli, G. 1988. The Middle Triassic magmatic–tectonic arc development in the Southern Alps. *Tectonophysics*, **146**, 79–89.
- Condon, D.J., Schoene, B., McLean, N.M., Bowring, S.A. & Parrish, R.R. 2015. Metrology and traceability of U–Pb isotope dilution geochronology (EARTHTIME Tracer Calibration Part I). *Geochimica et Cosmochimica Acta*, **164**, 464–480.
- De Lapparent, A.A. 1864. Memoire sur la constitution géologique du Tyrol méridional. *Annales des Mines ou Recueil de Mémoires sur l'Exploration des Mines, et sur les Sciences qui s'y rapportent: rédigés par le Conseil Général des Mines*. Paris, **6**, 245–314.
- De Vecchi, G. & Sede, R. 1983. Il vulcanesimo medio-triassico nelle Prealpi Vicentine (Italia sett.). *Memorie degli Istituti di Geologia e Mineralogia dell'Università di Padova*, **36**, 149–169.
- Ferry, J.M. & Watson, E.B. 2007. New thermodynamic models and revised calibrations for the Ti-in-zircon and Zr-in-rutile thermometers. *Contributions to Mineralogy and Petrology*, **154**, 429–437.
- Garzanti, E. 1985. The sandstone memory of the evolution of a Triassic volcanic arc in the Southern Alps, Italy. *Sedimentology*, **32**, 423–433.
- Gasparotto, G. & Simboli, G. 1991. Mineralogia, petrografia e schemi evolutivi delle magmatiti triassiche del complesso di Cima Pape (Dolomiti Orientali). *Mineralogica et Petrographica Acta*, **34**, 205–234.
- Gerstenberger, H. & Haase, G. 1997. A highly effective emitter substance for mass spectrometric Pb isotope ratio determinations. *Chemical Geology*, **136**, 309–312.
- Gianolla, P., De Zanche, V. & Mietto, P. 1998. Triassic sequence stratigraphy in the Southern Alps (Northern Italy): definition of sequences and basin evolution. In: de Graciansky, P.C., Hardenbol, J., Jacquin, T. & Vail, P.R. (eds) *Mesozoic and Cenozoic Sequence Stratigraphy of European Basins*. SEPM, Special Publications, **60**, 719–747.
- Glazner, A.F. & Sadler, P.M. 2016. Estimating the duration of geologic intervals from a small number of age determinations: a challenge common to petrology and paleobiology. *Geochemistry, Geophysics, Geosystems*, **17**, 4892–4898.
- Grimes, C.B., Wooden, J.L., Cheadle, M.J. & John, B.E. 2015. 'Fingerprinting' tectono-magmatic provenance using trace elements in igneous zircon. *Contributions to Mineralogy and Petrology*, **170**, 46.
- Guillong, M., von Quadt, A., Sakata, S., Peytcheva, I. & Bachmann, O. 2014. LA-ICP-MS Pb–U dating of young zircons from the Kos–Nisyros volcanic centre, SE Aegean arc. *Journal of Analytical Atomic Spectrometry*, **29**, 963–970.
- Hies, J., Condon, D.J., McLean, N. & Noble, S.R. 2012. $^{238}\text{U}/^{235}\text{U}$ systematics in terrestrial uranium-bearing minerals. *Science*, **335**, 1610–1614.
- Jadoul, F., Berra, F. et al. 2012. *Note Illustrative della Carta Geologica d'Italia alla scala 1: 50.000, Foglio 077 Clusone*. ISPRA, Servizio Geologico d'Italia.
- Jaffey, A.H., Flynn, K.F., Glendenin, L.E., Bentley, W.T. & Essling, A.M. 1971. Precision measurement of half-lives and specific activities of U-235 and U-238. *Physical Reviews*, **C4**, 1889–1906.
- Jagoutz, O. & Schmidt, M.W. 2012. The formation and bulk composition of modern juvenile continental crust: the Kohistan arc. *Chemical Geology*, **298–299**, 79–96.
- Jagoutz, O. & Schmidt, M.W., 2013. The composition of the foundered complement to the continental crust and a re-evaluation of fluxes in arcs. *Earth and Planetary Science Letters*, **371**, 177–190.
- Jagoutz, O., Müntener, O., Schmidt, M.W. & Burg, J.-P. 2011. The roles of flux- and decompression melting and their respective fractionation lines for continental crust formation: evidence from the Kohistan arc. *Earth and Planetary Science Letters*, **303**, 25–36.
- Keller, C.B., Schoene, B. & Samperton, K.M. 2018. A stochastic sampling approach to zircon eruption age interpretation. *Geochemical Perspectives Letters*, **8**, 31–35.
- Krogh, T.E. 1973. A low-contamination method for hydrothermal decomposition of zircon and extraction of U and Pb for isotopic age determinations. *Geochimica et Cosmochimica Acta*, **37**, 485–494.
- Large, S.J.E., von Quadt, A., Wotzlaw, J.-F., Guillong, M. & Heinrich, C.A. 2018. Magma evolution leading to porphyry Au–Cu mineralization at the Ok Tedi deposit, Papua New Guinea: trace element geochemistry and high-precision geochronology of igneous zircon. *Economic Geology*, **113**, 39–61.
- Masch, L. & Huckenholz, H. 1993. Der Intrusivkomplex von Monzoni und seine thermometamorphe Aureole. *European Journal of Mineralogy*, **5**, 81–135.
- Mattinson, J.M. 2005. Zircon U–Pb chemical abrasion ('CA-TIMS') method: combined annealing and multi-step partial dissolution analysis for improved precision and accuracy of zircon ages. *Chemical Geology*, **220**, 47–66.
- Mattinson, J.M. 2010. Analysis of the relative decay constants of ^{235}U and ^{238}U by multi-step CA-TIMS measurements of closed-system natural zircon samples. *Chemical Geology*, **275**, 186–198.
- McLean, N.M., Condon, D.J., Schoene, B. & Bowring, S.A. 2015. Evaluating uncertainties in the calibration of isotopic reference materials and multi-element isotopic tracers (EARTHTIME Tracer Calibration Part II). *Geochimica et Cosmochimica Acta*, **164**, 481–501.
- Meen, J.K. 1987. Formation of shoshonites from calcalkaline basalt magmas: geochemical and experimental constraints from the type locality. *Contributions to Mineralogy and Petrology*, **97**, 333–351.
- Mietto, P., Manfrin, S. et al. 2012. The Global Boundary Stratotype Section and Point (GSSP) of the Carnian stage (Late Triassic) at Prati di Stuares/Stuares Wiesen section (Southern Alps, NE Italy). *Episodes*, **35**, 414–430.
- Miller, C., Thöni, M., Goessler, W. & Tessadri, R. 2011. Origin and age of the Eisenkappel gabbro to granite suite (Carinthia, SE Austrian Alps). *Lithos*, **125**, 434–448.
- Mundil, R., Brack, P., Meier, M., Rieber, H. & Oberli, F. 1996. High resolution U–Pb dating of Middle Triassic volcanics: time-scale calibration and verification of tuning parameters for carbonate sedimentation. *Earth and Planetary Science Letters*, **141**, 137–151.
- Mundil, R., Zühlke, R. et al. 2003. Cyclicity in Triassic platform carbonates: synchronizing radio-isotopic and orbital clocks. *Terra Nova*, **15**, 81–87.
- Müntener, O. & Ulmer, P. 2018. Arc crust formation and differentiation constrained by experimental petrology. *American Journal of Science*, **318**, 64–89.
- Obenholzer, J.H. 1991. Triassic volcanogenic sediments from the Southern Alps (Italy, Austria, Yugoslavia)—a contribution to the 'Pietra verde' problem. *Sedimentary Geology*, **74**, 157–171.
- Pisa, G., Castellarin, A., Lucchini, F., Rossi, P.L., Simboli, G., Bosellini, A. & Sommariva, E. 1980. Middle Triassic magmatism in Southern Alps. I. A review of general data in the Dolomites. *Rivista Italiana di Paleontologia e Stratigrafia*, **85**, 1093–1110.
- Rioux, M., Bowring, S., Cheadle, M. & John, B. 2015. Evidence for initial excess ^{231}Pa in mid-ocean ridge zircons. *Chemical Geology*, **397**, 143–156.
- Russo, F., Neri, C., Mastandrea, A. & Baracca, A. 1997. The mud mound nature of the Cassian platform margins of the Dolomites. A case history: the Cipit boulders from Punta Grohmann (Sasso Piatto Massif, northern Italy). *Facies*, **36**, 25–36.
- Sacerdoti, M. & Sommariva, E. 1962. Pillowlave, ialoclastiti e altre formazioni vulcanoclastiche nella regione dolomitica occidentale. *Studi Trentini di Scienze naturali*, **39**, 423–473.
- Samperton, K.M., Schoene, B., Cottle, J.M., Keller, C.B., Crowley, J.L. & Schmitz, M.D. 2015. Magma emplacement, differentiation and cooling in the middle crust: integrated zircon geochronological–geochemical constraints from the Bergell Intrusion, Central Alps. *Chemical Geology*, **417**, 322–340.
- Schmitt, A.K. 2007. Ion microprobe analysis of (^{231}Pa)/(^{235}U) and an appraisal of protactinium partitioning in igneous zircon. *American Mineralogist*, **92**, 691–694.
- Schmitt, A.K., Konrad, K. et al. 2017. $^{40}\text{Ar}/^{39}\text{Ar}$ ages and zircon petrochronology for the rear arc of the Izu–Bonin–Marianas intra-oceanic subduction zone. *International Geology Review*, **60**, 956–976.
- Schoene, B., Crowley, J.L., Condon, D.J., Schmitz, M.D. & Bowring, S.A. 2006. Reassessing the uranium decay constants for geochronology using ID-TIMS U–Pb data. *Geochimica et Cosmochimica Acta*, **70**, 426–445.
- Schoene, B., Schaltegger, U., Brack, P., Lattkoczy, C., Stracke, A. & Günther, D. 2012. Rates of magma differentiation and emplacement in a ballooning pluton recorded by U–Pb TIMS-TEA, Adamello batholith, Italy. *Earth and Planetary Science Letters*, **355**, 162–173.
- Simon, J.I., Renne, P.R. & Mundil, R. 2008. Implications of pre-eruptive magmatic histories of zircons for U–Pb geochronology of silicic extrusions. *Earth and Planetary Science Letters*, **266**, 182–194.
- Spadea, P. 1970. Le ignimbriti riolitiche del membro superiore delle Vulcaniti di Rio Freddo, nel Trias medio della regione di Travisio (Alpi Giulie Occidentali). *Edizioni del Museo Trentino di Scienze Naturali*, **47**, 287–358.
- Stockar, R., Baumgartner, P.O. & Condon, D. 2012. Integrated Ladinian bio-chronostratigraphy and geochronology of Monte San Giorgio (Southern Alps, Switzerland). *Swiss Journal of Geosciences*, **105**, 85–108.
- Szymanowski, D., Fehr, M.A. et al. 2018. Isotope-dilution anchoring of zircon reference materials for accurate Ti-in-zircon thermometry. *Chemical Geology*, **481**, 146–154.
- von Quadt, A., Wotzlaw, J.-F., Buret, Y., Large, S.J., Peytcheva, I. & Trinquier, A. 2016. High-precision zircon U/Pb geochronology by ID-TIMS using new 10^{13} ohm resistors. *Journal of Analytical Atomic Spectrometry*, **31**, 658–665.
- Wier, J.F. 1997. Vergleichende Untersuchungen an Megasporenvergesellschaftungen der alpinen und germanischen Mittel- und Obertrias. *Münchner Geowissenschaftliche Abhandlungen, A, Geologie und Paläontologie*, **35**, 1–175.
- Wotzlaw, J.F., Schaltegger, U., Frick, D.A., Dungan, M., Gerdes, A. & Günther, D. 2013. Tracking the evolution of large-volume silicic magma reservoirs from assembly to supereruption. *Geology*, **41**, 867–870.

- Wotzlaw, J.F., Hüsling, S.K., Hilgen, F.J. & Schaltegger, U. 2014. High-precision zircon U–Pb geochronology of astronomically dated volcanic ash beds from the Mediterranean Miocene. *Earth and Planetary Science Letters*, **407**, 19–34.
- Wotzlaw, J.F., Buret, Y., Large, S.J., Szymanowski, D. & von Quadt, A. 2017. ID-TIMS U–Pb geochronology at the 0.1‰ level using $10^{13} \Omega$ resistors and simultaneous U and $^{18}\text{O}/^{16}\text{O}$ isotope ratio determination for accurate UO_2 interference correction. *Journal of Analytical Atomic Spectrometry*, **32**, 579–586.
- Wotzlaw, J.F., Brack, P. & Storck, J.-C. 2018. High-resolution stratigraphy and zircon U–Pb geochronology of the Middle Triassic Buchenstein Formation (Dolomites, northern Italy): precession-forcing of hemipelagic carbonate sedimentation and calibration of the Anisian–Ladinian boundary interval. *Journal of the Geological Society, London*, **175**, 71–85, <https://doi.org/10.1144/jgs2017-052>
- Zanetti, A., Giovanardi, T., Langone, A., Tiepolo, M., Wu, F.-Y., Dallai, L. & Mazzucchelli, M. 2016. Origin and age of zircon-bearing chromitite layers from the Finero phlogopite peridotite (Ivrea–Verbano Zone, Western Alps) and geodynamic consequences. *Lithos*, **262**, 58–74.